THE GEOLOGICAL SOCIETY OF AMERICA®

A 100-m.y.-long window onto mass-flow processes in the Patagonian Mesozoic subduction zone (Diego de Almagro Island, Chile)

Samuel Angiboust[1,†], Aitor Cambeses[1,2,†], Thais Hyppolito[3,†], Johannes Glodny[4,†], Patrick Monié[5,†], Mauricio Calderón[6,†], and Caetano Juliani[3]

[1]*Institut de Physique du Globe de Paris, Sorbonne Paris Cité, Université Paris Diderot, Centre National de la Recherche Scientifique (CNRS), F-75005 Paris, France*

[2]*Department of Mineralogy and Petrology, Faculty of Sciences, University of Granada, Campus Fuentenueva s/n, 18002 Granada, Spain*

[3]*Instituto de Geociências, Universidade de São Paulo, Rua do Lago, 562, 05505-080, São Paulo, Brazil*

[4]*German Research Centre for Geosciences (GFZ), 14473 Potsdam, Germany*

[5]*Géosciences Montpellier UMR-CNRS 5243, Place E. Bataillon, 34090 Montpellier, France*

[6]*Carrera de Geología, Universidad Andres Bello, Sazie 2119, Santiago, Chile*

ABSTRACT

Diego de Almagro Island was formed by the subduction and accretion of several seafloor-derived tectonic slices with very heterogeneous ages and pressure-temperature-time (*P-T-t*) paths. The highest element of the pile (the Lazaro unit) evidences subduction in the high-*P* granulite field (~1.3 GPa, 750 °C) at ca. 163 Ma. Below it, a thin tectonic sliver (the Garnet Amphibolite unit) preserves eclogite-facies remnants (~570 °C and ~1.7 GPa) formed at ca. 131 Ma (in situ U-Pb zircon rim ages). Peak assemblages were nearly fully amphibolitized during decompression down to ~1.2 GPa and ~600 °C at 125–120 Ma (Rb-Sr multimineral dating). The underlying Blueschist unit has ~50 m.y. younger metamorphic ages and exhibits slightly cooler peak burial conditions (~520 °C, 1.7 GPa; ca. 80 Ma, in situ white mica Ar-Ar ages and multimineral Rb-Sr dating) and is devoid of amphibolitization. The mylonites from the sinistral strike-slip Seno Arcabuz shear zone bounding Diego de Almagro Island to the east also exhibit amphibolite-facies (~620 °C and ~0.9 GPa) deformation at ca. 117 Ma (multimineral Rb-Sr ages). In situ white mica Ar-Ar dating and multimineral Rb-Sr dating of low-*T* mylonites (~450 °C) along the base of the Lazaro unit reveal partial resetting of high-*T* assemblages during tectonic displacement between 115 and 72 Ma and exhumation of the slice stack.

Detrital zircon U-Th-Pb ages indicate that the material accreted on Diego de Almagro Island has been mostly recycled from a Permian–Triassic accretionary wedge (Madre de Dios accretionary complex) exposed along the subduction buttress. Geological and geochronological constraints suggest that the rocks of the Seno Arcabuz shear zone and the Lazaro unit were tectonically eroded from the buttress, while the underlying Garnet Amphibolite and Blueschist units instead derive from the subducted oceanic basin, with increasingly younger maximum depositional ages. The very long residence time of the rocks (~90 m.y. for the Lazaro unit) along the hanging wall of the subduction interface recorded long-term cooling along the Patagonian subduction zone during the Mesozoic. Diego de Almagro Island therefore represents a unique window onto long-term tectonic processes such as subduction interface down-stepping, tectonic erosion, and episodic underplating near the base of an accretionary wedge (40–50 km).

INTRODUCTION

Exhumed metamorphic high-pressure–low-temperature (HP-LT) complexes provide an opportunity to understand the deep structure of present-day subduction zones between 30 and 80 km depth (e.g., Ernst and Dal Piaz, 1978; Cloos and Shreve, 1988; Ring and Brandon, 1999). Exhumation is a transient and discontinuous process over the duration of an entire subduction event (e.g., Maruyama et al., 1996; Agard et al., 2009). Although large volumes of oceanic lithosphere may be coherently exhumed after detachment from the downgoing plate (40–70 km along strike; Angiboust et al., 2009), such a rare event likely represents a perturbation in the normal subduction regime, which normally does not involve steady-state return flow of material back to near-surface conditions. In other words, only a very small fraction of the total subducted oceanic material escapes from subduction in the mantle via decoupling from the slab and a subsequent forced return flow and accretion to the upper plate ("underplating"; e.g., Platt, 1983; Ring and Layer, 2003). Field studies reveal that the depth range 30–40 km is particularly prone to underplating and stacking of crustal slices of continental and oceanic affinities (Willner et al., 2004a; Angiboust et al., 2014; Plunder et al., 2015). Multiple accretion events are believed to trigger the formation of crustal-scale duplex systems, where tectonic slices are vertically transported through the forearc crust, and up to the surface in some rare cases (e.g., Willner, 2005; Glodny et al., 2005; Konstantinovskaya and Malavieille, 2011). Despite the importance of tectonic processes taking place in the 30–40 km depth region (e.g., slow-slip events, base of the seismogenic zone, "transition zone"), the mechanisms controlling transient underplating processes are only partially understood. Since the resolution of geophysical seismic and tomographic images in this depth range hampers the observation of bodies thinner than ~2 km (e.g., Rondenay et al., 2008; Hilairet and Reynard, 2009), field studies on exhumed HP-LT complexes are crucial to improve our understanding of the structure of the subduction hanging wall in this region of the interface.

The southern Chilean subduction zone represents an interesting target because subduction

[†]angiboust@ipgp.fr, cambeses@ipgp.fr, thahyppolito@gmail.com, glodnyj@gfz-potsdam.de, patrick.monie@gm.univ-montp2.fr, mccaldera@gmail.com.

 https://doi.org/10.1130/B31891.1; 10 figures; 1 table; Data Repository item 2018101.

has proceeded (nearly) continuously since Paleozoic times along the SW margin of the South American plate (formerly the SW Gondwana margin; e.g., Hervé, 1988). The HP-LT tectonic sequence forming the fossil accretionary system ("the Western Series") corresponds to a continuous, ~2500-km-long metamorphic belt where oceanic rocks were accreted by basal accretion to the upper plate toward the end of the Paleozoic (e.g., Kato, 1985; Glodny et al., 2005; Willner et al., 2005, 2009). Younger, Mesozoic segments from the base of this paleo–accretionary wedge have been reported and studied further south on Diego de Almagro Island, a remote island in Chilean Patagonia (Fig. 1; Hervé and Fanning, 2002; Willner et al., 2004a). Recent investigations have shown that this island consists of a stack of slices of oceanic crust underplated at ca. 160 Ma, ca. 120 Ma, and ca. 80 Ma and metamorphosed under very different thermal gradients (Hyppolito et al., 2016; Angiboust

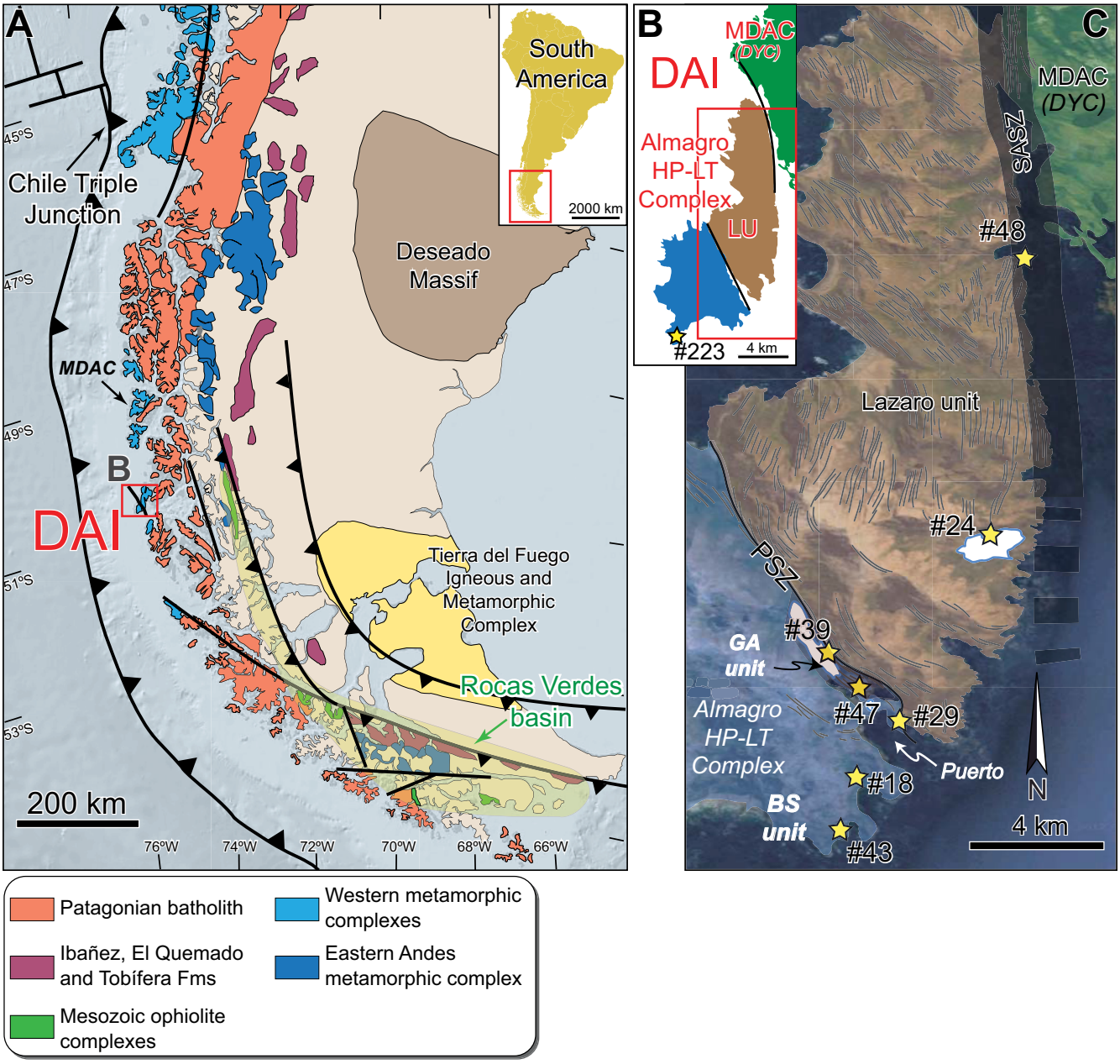

Figure 1. Geological map of the units forming Diego de Almagro Island. (A) Location of Diego de Almagro Island and Paleozoic and Mesozoic igneous and metamorphic complexes in Patagonia (modified form Hervé et al., 2007; Calderón et al., 2016). (B) Simplified geological map of the island showing the main units forming the Diego de Almagro metamorphic complex. DAI—Diego de Almagro Island, LU—Lazaro unit, AMC—Almagro high-pressure–low-temperature (HP-LT) metamorphic complex, SASZ—Seno Arcabuz shear zone, MDAC—Madre de Dios accretionary complex, DYC—Duke de York complex. (C) Detail of the Diego de Almagro metamorphic complex showing the contacts between the different units: the Puerto shear zone (PSZ) and the sinistral strike-slip Seno Arcabuz shear zone. BS—Blueschist unit; GA—Garnet Amphibolite unit. Stars are studied sample locations (global positioning system [GPS] coordinates given in Table DR4 [see footnote 1]).

et al., 2017). Some slivers forming Diego de Almagro Island reached depths greater than the base of the accretionary wedge (>40 km) and therefore possibly represent remnants from a paleo–subduction channel that were later basally accreted (Hyppolito et al., 2016). Yet, a unifying tectonic model that reconstructs the emplacement of these slices along the interface, as well as their individual tectonic histories, is missing. Further geochronological and pressure-temperature (*P-T*) constraints are herein provided to better understand the age distribution at the scale of the island and the migration of deformation along the major shear zones identified in the field. Zircon age distribution patterns were used to track the source and the fate of subducted material and therefore improve our vision of deformation processes rooted at the base of the accretionary wedge. We demonstrate why Diego de Almagro Island provides a unique record of the long-term geological evolution of the SW Gondwana margin in Patagonia across the entire Mesozoic Era.

REGIONAL GEOLOGICAL SETTING

The Chilean Coastal Cordillera, composed of late Paleozoic and Mesozoic subduction complexes, crops out between latitudes 28°S and 55°S and was formed via basal and frontal accretionary processes at the southwestern margin of the Gondwana continent (Kato, 1985; Hervé, 1988; Glodny et al., 2005; Willner, 2005). Most of these rocks reached high-pressure greenschist-facies conditions during late Paleozoic subduction, but only three occurrences exhibit rocks that reached slightly deeper peak burial conditions in the albite-epidote-amphibolite facies (~40 km), with evidence for counterclockwise pressure-temperature-time (*P-T-t*) paths (Los Pabilos—Willner et al., 2004b; Kato et al., 2008; Punta Sirena—Willner et al., 2005; Hyppolito et al., 2014; Los Caldos—Willner et al., 2012). Rare exposures of the Mesozoic accretionary complexes formed during the subduction of the proto-Pacific seafloor under the west Gondwana margin occur further south (46–55°S), flanking the western edge of the South Patagonian Batholith (Fig. 1; Madre de Díos, Diego de Almagro, and Diego Ramirez complexes; Mpodozis and Forsythe, 1983; Mpodozis and Ramos, 1990; Willner et al., 2004a, 2009; Charrier et al., 2007). The South Patagonian Batholith represents a composite assemblage of granitic plutons that were emplaced between 155 and 15 Ma across the Patagonian forearc (Fig. 1A; Hervé et al., 2007). Hervé et al. (2007) have shown that the position of pluton emplacement migrated toward the west between 144 and 127 Ma. The Madre de Dios accretionary complex comprises an actinolite-pumpellyite-facies accretionary prism that is exposed over several hundreds of kilometers, west of the South Patagonian Batholith (Fig. 1B). The Madre de Dios accretionary complex, which exhibits very low-grade metamorphism (290–310 °C and 0.4–0.6 GPa) and upper-crustal deformation style, has been interpreted by Willner et al. (2009) as a frontally accreted wedge. It is composed of a continent-derived detrital succession (Duque de York complex) tectonically interleaved with slices of oceanic crust (enriched [E] and normal [N] mid-ocean-ridge basalt [MORB], radiolarian and metalliferous cherts, pelites, and calcarenites) and platform carbonates (Forsythe and Mpodozis, 1983; Hervé et al., 1999; Sepúlveda et al., 2008). Ar-Ar ages from phengite reveal a Triassic accretion stage (ca. 233 Ma; Willner et al., 2009), and zircon U-Pb data, combined with palynological associations, restrict the maximum depositional age of the Duque de York complex to Permian times (ca. 270 Ma; Sepúlveda et al., 2010). We herein focus on Diego de Almagro Island, which is located west of the Madre de Dios accretionary complex, and which corresponds to a younger segment of the Mesozoic Western metamorphic complex (Hervé et al., 1999; Fig. 1B).

GEOLOGICAL STRUCTURE OF DIEGO DE ALMAGRO ISLAND

Almagro HP-LT Complex

Diego de Almagro Island is formed by an ~150 km^2 fragment of the basis of the Jurassic and Cretaceous accretionary wedge (Fig. 1A; Hervé et al., 1999; Hervé and Fanning, 2002; Willner et al., 2004a; Hyppolito et al., 2016; Angiboust et al., 2017). The southwestern half of Diego de Almagro Island is formed by the Almagro HP-LT complex (Figs. 1B and 1C), which consists of N- and E-MORB–type mafic meta-tuffs and meta-pillow lavas of mid- to Late Jurassic protolith ages, with minor intercalations of metasediments (quartzites and pelitic schists; Hervé and Fanning, 2002; Olivares et al., 2003; Willner et al., 2004a; Hyppolito et al., 2016). Hyppolito et al. (2016) have shown that the Almagro HP-LT complex can be subdivided into two subunits: the Garnet Amphibolite unit in the Puerto de Almagro area, and the Blueschist unit, which forms the southwestern half of the island (Fig. 1C). Evidence for HP metamorphism has been largely erased by a pervasive retrograde greenschist-facies event (Willner et al., 2004a). Diego de Almagro Island is crosscut by a major, 50–100-m-thick, east-dipping shear zone: the Puerto shear zone, which delineates the base of the Lazaro unit (Figs. 1C and 2A; Hyppolito et al., 2016). Below the Puerto shear zone, bodies with relics of eclogite-facies metamorphism (~1.7 GPa and ~550 °C) and a strong amphibolite-facies overprint, in the Garnet Amphibolite unit, yield multimineral Rb-Sr ages of ca. 120 Ma, which are interpreted as dating the amphibolitization stage (Hyppolito et al., 2016). The Garnet Amphibolite unit overlies (and is locally tectonically imbricated with) rocks from the Blueschist unit, in which this amphibolite-facies overprint is absent (Fig. 2B). Significantly younger Rb-Sr deformation ages of ca. 80 Ma have been reported by Hyppolito et al. (2016) for the mafic rocks from the Blueschist unit, which were metamorphosed during subduction at ~1.6 GPa and ~520 °C.

Lazaro Unit

The Lazaro unit, on the eastern part of Diego de Almagro Island (Figs. 1B and 1C), exhibits seafloor-derived mafic and metasedimentary rocks subducted down to ~1.2 GPa and ~750 °C conditions at the transition to the high-pressure granulite facies (Angiboust et al., 2017). Field evidence points to widespread partial melting, migmatitization, and trondhjemite formation and segregation (Fig. 2C; Angiboust et al., 2017). Several orthogneissic samples from this unit were studied by Hervé et al. (1999), Hervé and Fanning (2002), and Willner et al. (2004a). It has also been proposed that an orthogneiss body exposed along the eastern side of the Lazaro unit may represent a granitic fragment tectonically eroded from the upper plate that has been lately juxtaposed with HP-LT metamorphic rocks during subduction (Hervé and Fanning, 2002). The U-Pb age range of 170–165 Ma obtained for zircon rims from this material has been interpreted as a record of presubduction, extension-related magmatism associated with the breakup of Gondwana during the Late Jurassic, which culminated with the formation of mafic oceanic-type crust (e.g., the Rocas Verdes Basin; Fig. 1A) at ca. 155 Ma in a back-arc position (Hervé and Fanning, 2002; Calderón et al., 2013). Angiboust et al. (2017) proposed, based on sensitive high-resolution ion microprobe (SHRIMP) U-Pb zircon ages and multimineral Sm-Nd dating, that these rims more likely relate to a granulite-facies metamorphic event (~18 °C/km) that affected the base of the accretionary wedge at ca. 162 Ma. The zircon age distribution pattern (n = 35) shows that the maximum depositional age for the Lazaro unit metasediment is around ca. 250 Ma (Angiboust et al., 2017). Rocks from the Lazaro unit have been extensively affected by HP-LT metamorphic recrystallization after the peak-*T* event, as shown by LT amphiboles after pargasitic horn-

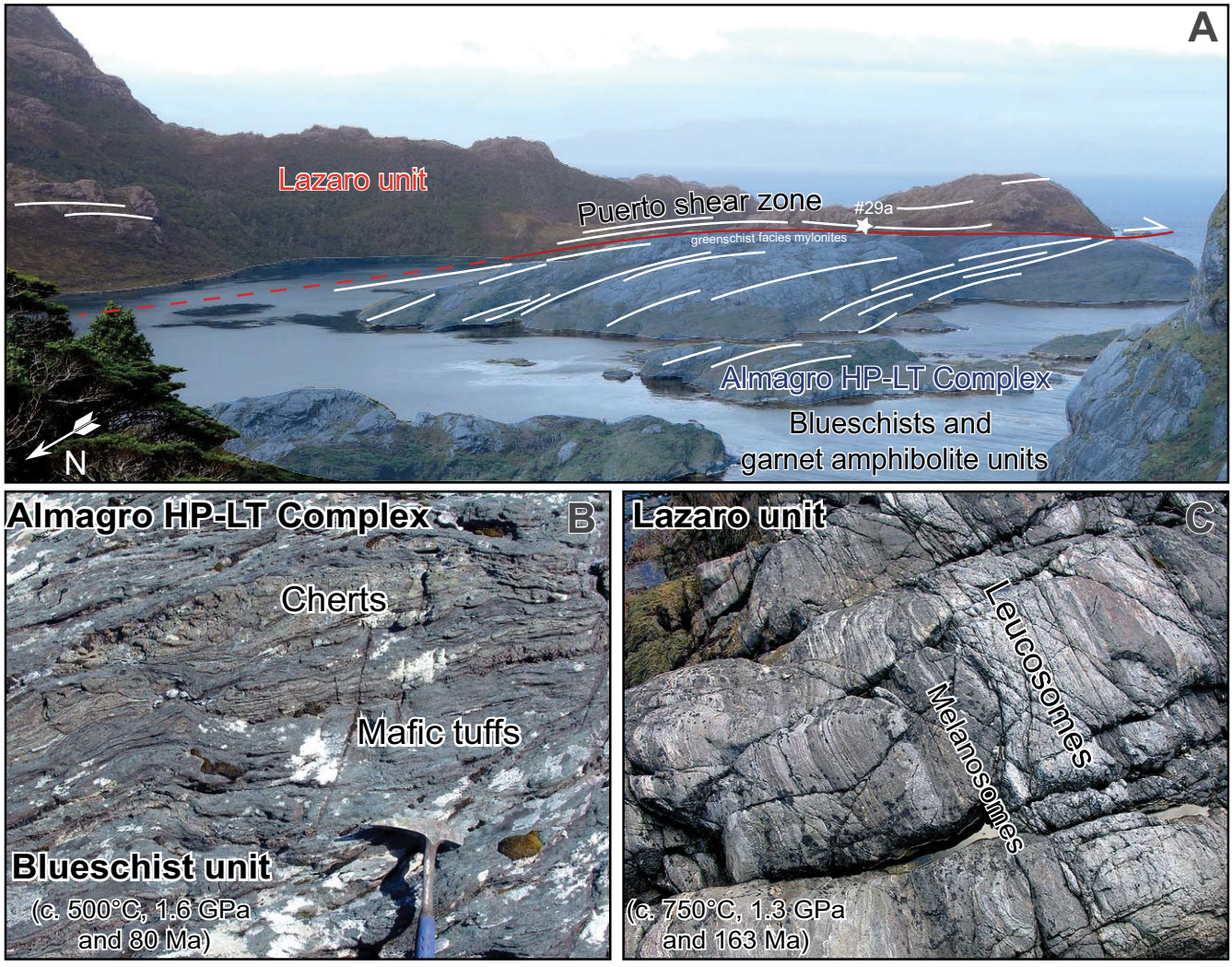

Figure 2. Field pictures of the Lazaro unit and Almagro high-pressure–low-temperature (HP-LT) complex. (A) Field photograph showing the contact between the Lazaro unit and the underlying HP-LT complex (Puerto shear zone). The star represents sample 29a location. (B) Representative Almagro HP-LT complex Blueschist unit outcrop showing the mafic tuff interlayered with cherts. (C) Lazaro unit outcrop containing numerous decimeter-thick strongly folded leucosomes and melanosomes (field of view: ~10 m). In both units, we indicate the conditions and ages of metamorphism.

blende and phengite rims around muscovite-rich cores (Angiboust et al., 2017; see also Willner et al., 2004a).

At least three deformation events can be identified in the Lazaro unit. A primary subvertical HT metamorphic foliation striking N-S to NE-SW and comprising numerous peritectic garnet crystals (related to partial-melting extraction processes) is crosscut by a series of NW-SE–striking, greenschist-facies shear zones subparallel to the main Puerto shear zone structure. In the lowermost hundred meters of the Lazaro unit (Fig. 2A; Hyppolito et al., 2016; Angiboust et al., 2017), the HT fabric has been transposed along the Puerto shear zone, leading to the formation of C-S greenschist-facies mylonites (e.g., sample 29a; Fig. 2A). Both top-to-the-NW kinematic indicators and back-shearing kinematic indicators have been observed along this thrust contact, which dips on average 20° to the SE. The upper part of the Garnet Amphibolite unit, along the Puerto shear zone, has been also affected by this LT mylonitic deformation stage. The eastern part of the Lazaro unit has been affected by a pervasive strike-slip mylonitic deformation stage along the Seno Arcabuz shear zone (see Fig. 1C and following text).

Seno Arcabuz Shear Zone

In the Diego de Almagro Island region, the Madre de Dios accretionary complex is bounded to the west by a multikilometer-thick sinistral, NNW-trending subvertical strike-slip shear zone, the Seno Arcabuz shear zone, along which mylonitic deformation caused partial reworking of the eastern part of Diego de Almagro Island and juxtaposition with the Madre de Dios accretionary complex (Fig. 1C; Hervé et al., 1999; Olivares et al., 2003; Willner et al., 2004a, 2009). The amphibolite-facies deformation stage visible in Seno Arcabuz shear zone rocks has been estimated to have at conditions around 580–690 °C and 0.5–0.6 GPa (Willner et al., 2004a). K-Ar dating of muscovite yielded an age of 122 ± 4.6 Ma for a garnet mica schist from the Seno Arcabuz shear zone (Willner et al., 2004a). The HT metamorphism along the Seno Arcabuz shear zone has been interpreted by Willner et al. (2004a) as evidence for heat advection associated with the coeval emplacement

of the magmatic arc as expected in a paired belt system where HP-LT and low-pressure–high-temperature (LP-HT) belts coexist.

The Seno Arcabuz shear zone consists of a subvertical sequence showing an alternation of very dark mafic schists and meter-thick metapelitic intervals. The mafic layers from the Seno Arcabuz shear zone mainly exhibit N-MORB signatures (raw data shown in Hyppolito, 2010). No sharp lithological and tectonic boundary has been identified in the field between the Seno Arcabuz shear zone and the eastern part of the Lazaro unit. Unlike in the adjacent Lazaro unit (Angiboust et al., 2017), no macroscopic evidence for trondhjemite genesis or partial melting is visible along the Seno Arcabuz shear zone. Ultramafic rocks have not been observed along this shear zone. At the microscopic scale, the mylonites from the Seno Arcabuz shear zone are characterized by a pervasive flattening, and by a relatively homogeneous grain-size diameter between 50 µm and 200 µm (see a full petrological description given as Data Repository Appendix DR1).[1] Plagioclase and hornblende "augen" are volumetrically rare (<1 vol% on average). Mafic layers are characterized by an alternation between hornblende- and plagioclase-rich layers aligned along the main N-S–striking foliation. Locally, layers richer in biotite and muscovite are visible (Data Repository Appendix DR1 [see footnote 1]). Garnet is extremely rare in mafic lithologies, while it is very common in metapelitic layers (Willner et al., 2004a). Staurolite porphyroclasts (100–300 µm long) are also present in pelitic or quartzofeldspathic lithologies associated with micas and garnet (Data Repository Appendix DR1 [see footnote 1]). Importantly, very thin phengite rims around muscovite cores, actinolitic rims around hornblende, and stilpnomelane needles in the matrix suggest that a HP-LT event statically overprinted the amphibolite-facies foliation (counterclockwise *P-T* path; see Willner et al., 2004a; see also microscopic images in Data Repository Appendix DR1 [footnote 1]).

ANALYTICAL METHODS

Rb-Sr Multimineral Geochronology

In order to provide age constraints for the timing of ductile deformation along the Seno Arcabuz shear zone, we investigated Rb-Sr multimineral isotope systematics in a mylonitic sample (48b; Fig. 1C) containing biotite and white mica. Isotopic data were obtained at the Deutsches GeoForschungsZentrum (GFZ) Potsdam, Germany, using a Thermo Scientific TRITON thermal-ionization mass spectrometer (TIMS). Rb isotope dilution analysis was done in static multicollection mode, and Sr isotopic composition was measured in dynamic multicollection mode. For $^{87}Sr/^{86}Sr$ isotopic compositions, we used the variance of values obtained from long-term reproducibility tests of the NBS SRM 987 reference material on the GFZ Potsdam TIMS mass spectrometer and applied an uncertainty of ±0.005%, provided that the individual analytical uncertainties were smaller than that value. Otherwise, measured analytical uncertainties were applied. The age uncertainty in isochron calculations is commonly (and in our case) dominated by uncertainties in Rb/Sr ratios. Based on reproducibility tests for $^{87}Rb/^{86}Sr$ ratios of spiked white mica samples, we applied a (conservative) estimate of ±1.5% for $^{87}Rb/^{86}Sr$ ratios. Mineral separation techniques and analytical procedures followed those described in detail in Glodny et al. (2008). Uncertainties of isotope and age data are quoted at a 2σ level. The program Isoplot/Ex 3.71 (Ludwig, 2009a) was used to calculate regression lines. We used the Rb decay constant recommended by Villa et al. (2015).

In Situ $^{40}Ar/^{39}Ar$ White Mica Dating

To establish the age of the metamorphic events in the different units from Diego de Almagro Island, we obtained $^{40}Ar/^{39}Ar$ in situ ages of: (1) three samples of the Almagro HP-LT complex (one from Garnet Amphibolite unit, 39c, and two from Blueschist unit, 223j and 18a; Figs. 1B and 1C), and (2) two samples from the Lazaro unit (24 and 29a; Fig. 1C). The $^{40}Ar/^{39}Ar$ in situ laser-ablation method was developed by Megrue (1973) and upgraded by York et al. (1981) and Maluski and Monié (1988) (see also McDougall and Harrison, 1999, and references therein). The five polished rock sections of 2 mm thickness and 1 cm^2 area were irradiated in the Triga Mark II nuclear reactor (Pavia, Italia) with several aliquots of the Fish Canyon sanidine standard as flux monitor. Measurements were performed at Geosciences Montpellier using (1) a pulsed ultraviolet laser of 100 kHz, (2) a lens system for beam focusing, (3) a camera connected to the monitor for beam focusing and selection of ablated zones, (4) a steel chamber with a copper plate where samples were loaded, (5) an inlet line for purification of gases, including two Zr-Al getters, (6) a multicollector mass spectrometer (Argus VI from Thermo-Fisher), and (7) software that controlled the timing of extraction/purification and the data acquisition. For each analysis, argon was released from an ablated zone of 200 µm diameter and 10–30 µm depth (ablation time: 4 min). The proportion of ^{38}Ar and ^{37}Ar isotopes that result from nuclear reactions with chlorine and calcium during irradiation reveals the contribution of Cl minerals/Cl-rich inclusions or Ca minerals/Ca-rich inclusions to the argon release and then to the calculated age. A blank analysis was done every three analyses to evaluate the argon background based on the algorithms described in Faure (1986), McDougall and Harrison (1999), and Min et al. (2000). Atmospheric ^{40}Ar was corrected using a value of initial $^{40}Ar/^{36}Ar$ of 295.5. Isotopic results were computed with the ArArCalc software (Koppers, 2002). The full analytical data set is presented in Table DR2 (see footnote 1), and the locations of spot analyses are provided in Data Repository Appendix DR2 (see footnote 1).

Zircon SHRIMP Analyses

Zircon crystals were separated from representative samples from: (1) the Almagro HP-LT complex: two from the Garnet Amphibolite unit (47a and 39) and one from the Blueschist unit (43); and (2) the Seno Arcabuz shear zone (48c; see sample location in Fig. 1C). The U-Th-Pb SHRIMP zircon analyses were performed at the Scientific Analytical Centre (Centro de Instrumentación Científica [CIC]), University of Granada, Spain. Zircon was separated using panning, first in water and then in ethanol. This was followed by magnetic extraction of Fe-rich minerals with a Nd magnet. Finally, zircon grains were handpicked using a binocular microscope. The zircon grains were cast on "mega-mounts," i.e., 35 mm epoxy discs fixed on the front of a mount holder so that no metallic parts or surface discontinuities faced the secondary ion extraction plate. The minerals were carefully studied with optical (reflected and transmitted light) and scanning electronic microscopy (backscattering and cathodoluminescence [CL]) prior to SHRIMP analyses with the IBERSIMS SHRIMP IIe/mc ion microprobe.

Zircon crystals were analyzed for U-Th-Pb following the method described by Williams and Claesson (1987). The mount was coated with an ~12-nm-thick gold layer. Each spot was rastered with the primary beam for 120 s prior to analysis and then analyzed for six scans following the isotope peak sequence: $^{196}Zr_2O$, ^{204}Pb, $^{204.1}$background, ^{206}Pb, ^{207}Pb, ^{208}Pb, ^{238}U, ^{248}ThO, and ^{254}UO. Every peak of every scan was measured sequentially 10 times with the following total counting times per scan: 2 s for mass 196; 5 s for masses 238, 248, and 254; 15 s for masses 204, 206, and 208; and 20 s

[1]GSA Data Repository item 2018101, full geochronological data set, global positioning system (GPS) coordinates, and petrological information on the Seno Arcabuz shear zone, is available at http://www.geosociety.org/datarepository/2018 or by request to editing@geosociety.org.

for mass 207. The primary beam, composed of $^{16}O^{-16}O^{+}$, was set to an intensity of ~5 nA, with two Köhler apertures: (1) at 120 µm and (2) at 70 µm, which generated 17 × 20 and 9 × 12 µm elliptical spots on the target, respectively. We used the small spot to obtain data in small areas in selected zircon, such as metamorphic rims. The secondary beam exit slit was fixed at 80 µm, achieving a resolution of ~5000 at 1% peak height. All calibration procedures were performed on the standards included on the same mount. Mass calibration was done on the REG zircon (ca. 2.5 Ga, with very high U, Th, and common Pb content). The analytical session started by measuring the SL13 zircon (Claoué-Long et al., 1995), which was used as a concentration standard (238 ppm U). The Temora I zircon (416.8 ± 1.1 Ma; Black et al., 2003), used as an isotope ratio standard, was then measured after every four unknowns. Data reduction was done with the SHRIMPTOOLS software (available from www.ugr.es/~fbea), which is a new implementation of the PRAWN software originally developed for the SHRIMP. Errors are reported at the 95% confidence interval (~2σ). Standard errors (95% confidence intervals) on the 37 replicates of the Temora standard measured during the analytical session were ±0.35% for $^{206}Pb/^{238}U$ and ±0.83% for $^{207}Pb/^{206}Pb$. The SHRIMP U-Th-Pb data are reported in Table DR3 (see footnote 1).

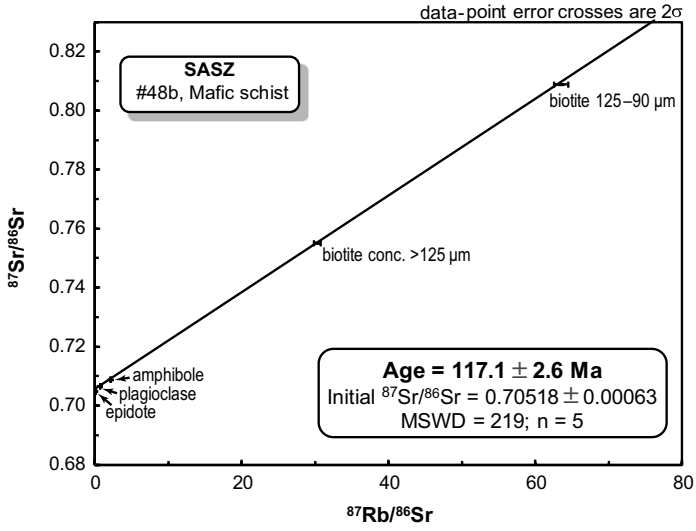

Figure 3. Rb-Sr analytical result from sample 48b, Seno Arcabuz shear zone (SASZ), for the mylonitization stage prevailing during high-temperature (HT) deformation in the amphibolite facies (~620 °C, 0.9 GPa). MSWD—mean square of weighted deviates.

GEOCHRONOLOGICAL RESULTS

Rb-Sr Geochronology

Mylonitic deformation events in mica-bearing metamorphic rocks can generally yield well-constrained multimineral Rb-Sr isochrons. Sr-isotopic re-equilibration and reset of ages are achieved via HT, deformation-induced recrystallization and re-equilibration of mineral phases (such as mica, albite, apatite, and titanite; e.g., Inger and Cliff, 1994; Angiboust et al., 2016). In the selected sample from the Seno Arcabuz shear zone (48b), two grain-size fractions of biotite were analyzed in order to detect potentially protracted recrystallization or deformation histories of the studied rocks (Fig. 3). In sample 48b, biotite is tightly intergrown with muscovite, and it is therefore likely that analyzed fractions correspond to mixtures of biotite with minor amounts of muscovite. This sample is particularly suited for Rb-Sr geochronology because the mylonitic fabric is very pervasive, and microscopic porphyroclasts (susceptible to yield disequilibrium patterns) are volumetrically rare (<1%). A relatively well-defined regression line, calculated combining two biotite fractions, hornblende, plagioclase, and epidote, yielded an age value of 117.1 ± 2.6 Ma (mean square of weighted deviates [MSWD] = 219). The reason for the elevated MSWD value is the slight but significant Sr-isotopic disequilibria between the low-Rb/Sr phases epidote, amphibole, and plagioclase. The calculated initial $^{87}Sr/^{86}Sr$ isotopic compositions for t = 117 Ma vary between 0.70473 (epidote) and 0.70546 (albite), with amphibole (0.70528) in between. This scatter is beyond analytical uncertainties and must have geologic reasons, either in the fluid-rock interaction history or in the metamorphic reaction history of the rock. Nevertheless, individual regression of the two biotite points with the data for the three low-Rb/Sr phases formally yielded ages between 118.0 Ma (epidote) and 116.7 Ma (albite), with each three-point regression yielding low MSWD (<1.7) isochron correlations. It appears that the age information is hardly sensitive to the observed initial Sr-isotopic disequilibria. We therefore regard the age estimate of 117.1 ± 2.6 Ma derived from the combined data set as accurately dating the mylonitic deformation stage that affected the Seno Arcabuz shear zone during sinistral strike-slip displacement (Fig. 3).

^{39}Ar-^{40}Ar Geochronology

The two selected samples from the Blueschist unit came from upper part and lower part of the unit, respectively: 18a and 223j (Fig. 4). The Garnet Amphibolite unit sample came from the core of the unit (39c; Figs. 1C and 4). Samples from the Lazaro unit were located in the center and base of that unit, respectively, 24 and 29a (Figs. 1C and 4). The results of more than 60 in situ analyses are shown in Figure 4, where obtained white mica ages are correlated with silica contents and microtextural position. A first event can be identified in samples 24 and 39c, where low-Si white mica cores exhibit variable ages between 110 and 125 Ma (Fig. 4). A second group of mica with a higher silica content that defines the main schistosity of these samples provides ages of 100 ± 3 Ma and 103 ± 5 Ma. This indicates that mica initially formed under amphibolite conditions remained unaffected during the HP-LT overprint. Conversely, a single well-defined metamorphic event is visible in the Blueschist unit sample 18a. In the two other samples (29a and 223j), the dispersion of ages between 60 and 80 Ma (Fig. 4) suggests the presence of small-scale heterogeneities, partial phengite recrystallization, and mixing of white mica core and rim domains during in situ laser ablation. Sample 29a from the Puerto shear zone at the base of the Lazaro unit displays six minimum ages of 70 ± 2 Ma, which mark the end of activity of this shear zone, while recrystallization proceeded until 60 Ma at the base of the Blueschist unit.

Zircon U-Th-Pb Geochronology

For some of the samples studied, the measured U-Th-Pb isotope systematics indicate discordance resulting from a common Pb contribution. We applied a ^{208}Pb-based correction algorithm (Ludwig, 2009b) that corrected the majority of data to concordia quite well and are virtually identical to ^{207}Pb-corrected data (Table DR3 [see footnote 1]). For geochrono-

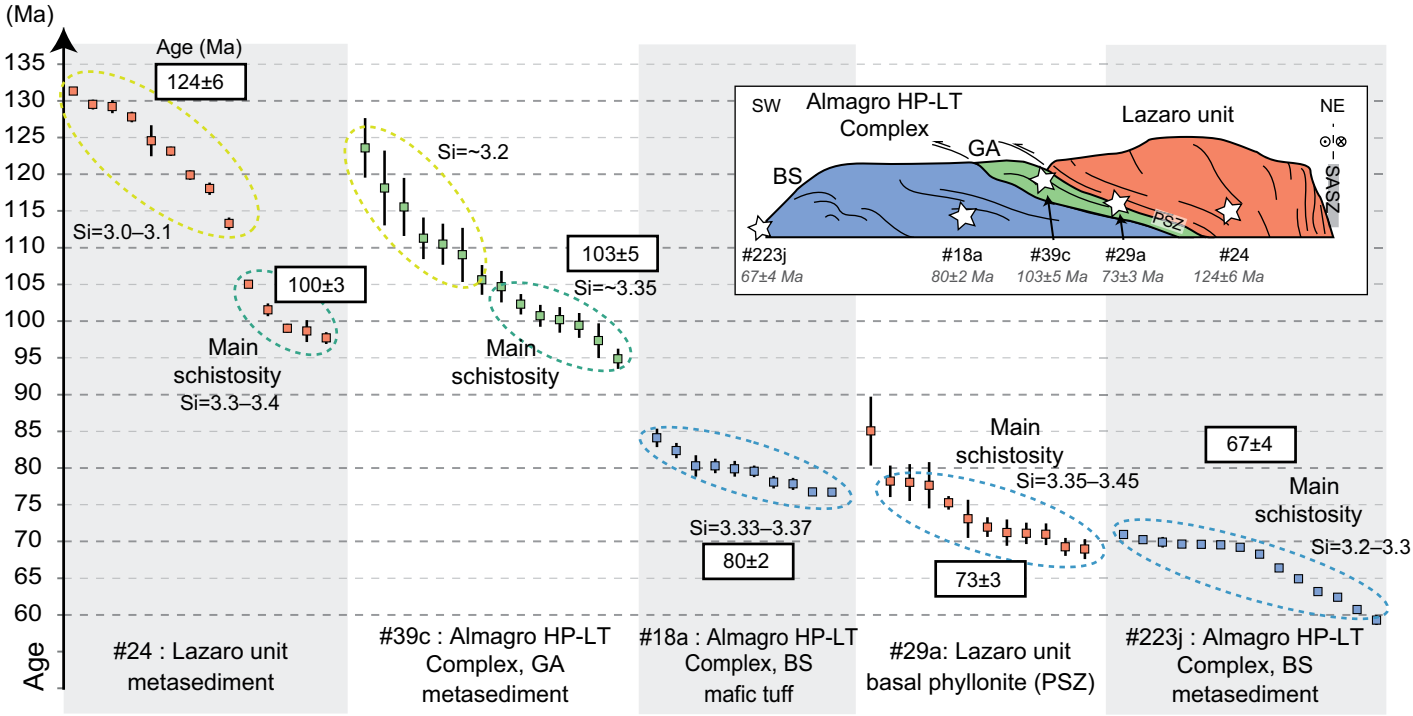

Figure 4. In situ white mica geochronological Ar-Ar age results from the Lazaro unit and the Almagro metamorphic complex. Location of studied samples is indicated in a simplified cross section (top right). Note the correlation of ages and Si content of white mica (muscovite and phengite; data from Hyppolito et al., 2016; Angiboust et al., 2017). Almagro HP-LT—Almagro high-pressure–low-temperature complex; BS—Blueschist unit; GA—Garnet Amphibolite unit; PSZ—Puerto shear zone; SASZ—Seno Arcabuz shear zone.

logical evaluation, we considered only data with discordance <±10% after correction of common Pb contributions (Fig. S1 [footnote 1]).

Seno Arcabuz Shear Zone

Sample 48 contained zircon grains with a wide range of sizes and morphologies. For this sample, we measured 79 spots, 55 of which resulted in concordant age information (Table DR3 [see footnote 1]). The ages obtained may be divided into three groups. The first group consists of Precambrian colorless rounded cores and thin rims, with a size of ~100 µm × 50 µm and oscillatory zoning pattern (Fig. 5A). Nineteen U-Th-Pb measurements on 19 zircon crystals yielded a wide $^{206}Pb/^{238}U$ age range, from Paleoproterozoic to Ediacaran, i.e., 1626–542 Ma (Figs. 5A and 6A). The second group consists of Paleozoic stubby ~75 µm × 50 µm grains with irregular terminations (Fig. 5A). Thirty-two U-Th-Pb measurements on 29 zircon crystals yielded $^{206}Pb/^{238}U$ ages from Cambrian to Permian, 538–253 Ma (Figs. 5A and 6A). The third group is Mesozoic in age. These zircon grains appear as ~100 µm × 50 µm prismatic crystals with oscillatory zoning and as small rims, ~30 µm × 15 µm (Fig. 5A). Four measurements, performed on four grains, gave Early to Middle Triassic, 249–235 Ma, $^{206}Pb/^{238}U$ ages (Figs. 5A and 6A). In this sample, late Paleozoic (Permian) and early Mesozoic (Triassic) ages formed a well-defined cluster (Fig. 6A). The weighted mean (n = 11, errors reported at 2σ) of the $^{206}Pb/^{238}U$ ages is 255 ± 8 Ma (MSWD = 4.88), and that of the $^{207}Pb/^{235}U$ ages is 261 ± 10 Ma (MSWD = 0.12; Fig. 6A).

Almagro HP-LT Complex, Garnet Amphibolite Unit

Sample 47A contained abundant zircon grains with a small range of sizes but very heterogeneous morphologies (Fig. 5B). For this sample, we measured 81 spots, 51 of which resulted in concordant age information (Table DR3 [see footnote 1]). The data may be divided into two groups based on the texture and the age of each grain. The first group included colorless to translucent bipyramid-terminated prisms to rounded grains. These grains, ~100 µm × 50 µm in size, comprised cores and scarce rims with oscillatory and patchy zoning (Fig. 5B). Twenty-eight U-Th-Pb measurements on 27 grains yielded $^{206}Pb/^{238}U$ Precambrian (1303–607 Ma), Paleozoic (534–259 Ma), and Mesozoic (181–172 Ma), ages (Figs. 5B and 6B). The second group included small, 40 µm × 20 µm, low-CL rims, all overgrowths on previous group zircon grains (Fig. 5B). Twenty-three U-Th-Pb measurements were carried out on 23 different grains and showed a $^{206}Pb/^{238}U$ age range of 138–124 Ma (Fig. 6B). The weighted mean (errors reported at 2σ, n = 23) of the $^{206}Pb/^{238}U$ ages is 131 ± 2 Ma (MSWD = 3.21), and that of the $^{207}Pb/^{235}U$ ages is 135 ± 2 Ma (MSWD = 0.05; Fig. 6B).

In sample 39, the grains had small sizes and heterogeneous morphologies. For this sample, we measured 48 spots, 27 of which yielded concordant age information (Table DR3 [see footnote 1]). Two groups were recognized based on textural and age criteria. The first group consisted of prismatic euhedral, ~125 µm × 50 µm grains with evidence for magmatic oscillatory zoning (Fig. 5C). Sixteen measurements on 16 grains were carried out and gave $^{206}Pb/^{238}U$ ages from Precambrian (1131–604 Ma), to Paleozoic (508–254 Ma), to Mesozoic (234–178 Ma; Figs. 5C and 6C). The second group was made up of rims that overgrew all previous zircon groups (Fig. 5C). These rims were thin, 30 µm × 15 µm, without visible internal structure (Fig. 5C). Eleven U-Th-Pb measurements performed on 11 different rims gave a $^{206}Pb/^{238}U$ age range of 140–120 Ma (Fig. 6C). The weighted mean (errors reported at 2σ, n = 11) of the $^{206}Pb/^{238}U$ ages is 132 ± 6 Ma (MSWD = 6.63), and that of the $^{207}Pb/^{235}U$ ages is 127 ± 4 Ma (MSWD = 0.14; Fig. 6C).

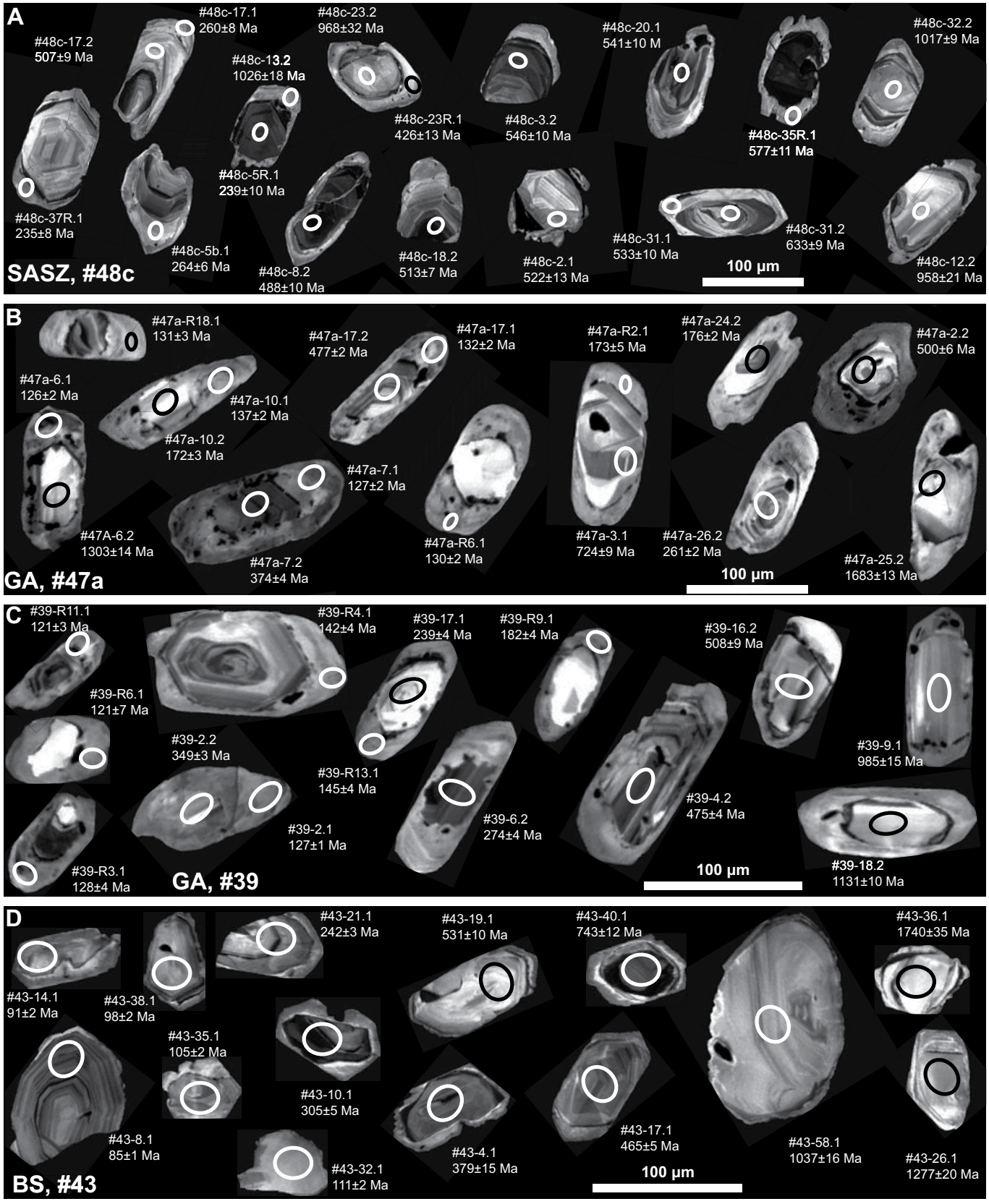

Figure 5. Cathodoluminescence images and ^{208}Pb-corrected $^{206}Pb/^{238}U$ ages of representative analyzed zircon grains from: (A) Seno Arcabuz shear zone (SASZ) sample 48c; (B) Almagro high-pressure–low-temperature (HP-LT) complex Garnet Amphibolite unit (GA) sample 47a and (C) GA sample 39; and (D) Almagro HP-LT complex Blueschist unit (BS) sample 43.

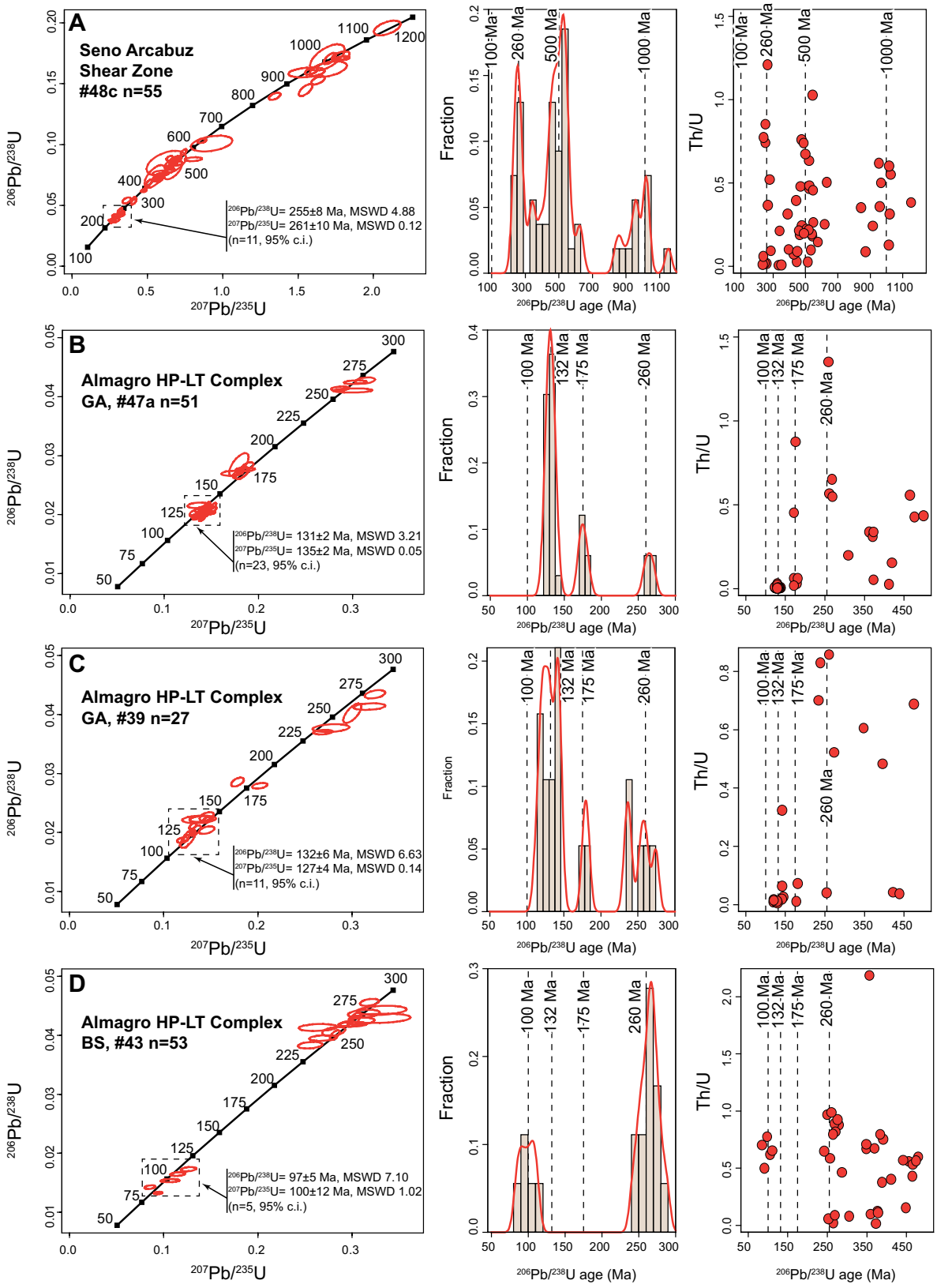

Figure 6. Wetherill concordia plots for frequency and density distribution and Th/U ratios of ^{208}Pb-corrected ^{206}Pb/^{238}U ages from: (A) Seno Arcabuz shear zone (SASZ) sample 48c; (B) Almagro high-pressure–low-temperature (HP-LT) complex Garnet Amphibolite unit (GA) sample 47a and (C) GA sample 39; and (D) Almagro HP-LT complex Blueschist unit (BS) sample 43. MSWD—mean square of weighted deviates; c.i.—confidence interval.

Almagro HP-LT Complex, Blueschist Unit

The grains from the Blueschist unit sample 43 (graphitic schist) presented heterogeneous sizes and morphologies. For this sample, we measured 58 spots, 53 of which resulted in concordant age information (Table DR3 [see footnote 1]). The ages obtained may be divided into three groups. The first group consisted of Precambrian colorless rounded cores and thin rims with size ~120 µm × 60 µm (Fig. 5D). Twelve U-Th-Pb measurements on 12 zircon crystals yielded a $^{206}Pb/^{238}U$ age range of 1740–579 Ma (Figs. 5D and 6D). The second group is made of Paleozoic stubby ~100 µm × 50 µm grains with prismatic and irregular terminations (Fig. 5D). Thirty-four U-Th-Pb measurements on 34 zircon grains gave $^{206}Pb/^{238}U$ ages from Cambrian to Permian, 539–253 Ma (Figs. 5D and 6D). The third group consisted of Mesozoic zircon crystals, with variable morphologies and sizes (~75 µm × 50 µm; Fig. 5D). Seven measurements, performed on 7 grains yielded a ^{208}Pb-corrected $^{206}Pb/^{238}U$ age range from Triassic to Late Cretaceous, 250–85 Ma (Fig. 6D). Younger zircon grains yielded a weighted mean (errors reported at 2σ, $n = 5$) $^{206}Pb/^{238}U$ age of 97 ± 5 Ma (MSWD = 7.10), and the weighted mean of $^{207}Pb/^{235}U$ ages was 100 ± 12 Ma (MSWD = 1.02; Fig. 6D). Last, most of the grains from sample 43 were surrounded by very thin rims (<10 µm width) that were too narrow to be analyzed (Fig. 5D). Notably, these rims are also present in Cretaceous zircon crystals and therefore likely correspond to a zircon growth event younger than ca. 100 Ma.

DISCUSSION

Interpretation of Zircon Ages

Zircon Provenance Analysis and Tectonic Implications

Premetamorphic zircon age patterns were evaluated here in order to trace the source of sediments forming the protoliths of accreted metamorphic units of Diego de Almagro Island and the relation with other metamorphic complexes in the Patagonian Andes. We compiled a data set of potential basement sources of south Chilean metamorphic complexes (cf. Hervé et al., 2007, 2006), including Ordovician to Permian igneous rocks and Cambrian–Ordovician and Late Triassic–Early Permian metasedimentary rocks from the Deseado and Somun Cura massifs (Fig. 7A; Pankhurst et al., 2003, 2006; Moreira et al., 2013). For comparison, we also added to this database the Late Devonian to Early Triassic metasedimentary rocks from comparable metamorphic complexes of southern Chile: the Eastern Andes, Main Range, and Chonos metamorphic complexes and the Duque de York complex (Fig. 7B; Hervé and Fanning, 2001; Hervé et al., 2003; Augustsson et al., 2006; Sepúlveda et al., 2010; Calderón et al., 2016). In addition, we completed the database with available U-Th-Pb zircon ages of metamorphic rocks from the Lazaro unit and Almagro HP-LT complex forming Diego de Almagro Island (Figs. 7C–7E; Hervé and Fanning, 2002; Angiboust et al., 2017).

The U-Th-Pb zircon ages from pre-Jurassic zircon grains older than 200 Ma in the different units forming Diego de Almagro Island have a broadly comparable distribution, with abundant Triassic to late Carboniferous ages (310–200 Ma), Middle Devonian to Cambrian zircon crystals (540–360 Ma), minor Neoproterozoic Ediacaran to Cryogenian ages (790–580 Ma), and Neoproterozoic (Tonian) to Mesoproterozoic (Stenian) ages (1160–920 Ma; Figs. 7C–7E). Given this zircon age pattern, we consider that there was a similar provenance source for pre-Jurassic zircon crystals for the different metamorphic units forming Diego de Almagro Island. Other metamorphic complexes of southern Chile exhibit zircon age distribution patterns that are fairly similar, with Triassic to late Carboniferous, Middle Devonian to Cambrian, Neoproterozoic, and Mesoproterozoic ages (Fig. 7B; cf. Hervé and Fanning, 2001; Hervé et al., 2003; Augustsson et al., 2006; Sepúlveda et al., 2010). The provenance of Cambrian to Permian zircon crystals is attributed to the granitic intrusions (540–290 Ma) in eastern Patagonia, which are well exposed in the Somun Cura and Deseado massifs (Fig. 7A; Pankhurst et al., 2003, 2006). Neoproterozoic and Mesoproterozoic detrital zircon grains have been related to a Patagonian origin, with a minor contribution from cratonic areas such as the Sao Francisco, Brazil, or the Rio de la Plata, Uruguay, i.e., Gondwana cratons (e.g., Hervé et al., 2003; Augustsson et al., 2006).

Hervé et al. (2003) have shown that the variable maximum depositional age range of metasedimentary rocks from metamorphic complexes of southern Chile spans Early Triassic to Late Permian, 280–240 Ma (Fig. 7B; e.g., Augustsson et al., 2006; Sepúlveda et al., 2010). The maximum depositional age of the Duque de York complex, 289–272 Ma (Hervé et al., 2003; Sepúlveda et al., 2010; Castillo et al., 2016), is older than the maximum sedimentation cluster age of sample 48c from the Seno Arcabuz shear zone (ca. 255 Ma; present work) and that for the Lazaro unit (ca. 251 Ma; Angiboust et al., 2017; Figs. 7B–7E). This ca. 255 Ma age cluster is also recognizable in Almagro HP-LT complex samples (Figs. 7B–7E), although a younger maximum sedimentation age has been identified (see following). The absence of younger detrital zircon grains in sample 48c from the Seno Arcabuz shear zone and samples from the Lazaro unit (sample 24 from Angiboust et al., 2017; sample AL12 from Hervé and Fanning, 2002), as well as their zircon age distributions (see Electronic Appendix DR3 [see footnote 1] for a Cawood cumulative diagram), suggests that this sample is derived from the adjacent Permian–Triassic Madre de Dios accretionary complex, part of the Duque de York complex (Figs. 1B and 1C).

Based on similar zircon age distribution and bulk-rock geochemistry, and considering that the high-temperature–medium-pressure (HT-MP) overprint recorded by the Seno Arcabuz shear zone and Lazaro unit samples is absent from Madre de Dios accretionary complex lithologies, we propose that coherent, shallow fragments of the Permian–Triassic wedge were tectonically eroded during the early Mesozoic and subducted down to ~35 km depth (the protolith of the Seno Arcabuz shear zone) and beyond (Lazaro unit). Such an erosive mechanism is a common process along the Chilean margin, and it is generally interpreted as reflecting changes in subduction coupling (e.g., seamount subduction) or as related to a decrease in sediment influx into the trench (e.g., Von Huene and Lallemand, 1990; Kukowski and Oncken, 2006). The finding of a similar zircon population signature in all Diego de Almagro Island tectonic units also confirms that the frontally accreted Permian–Triassic Madre de Dios accretionary complex wedge remained in a buttress position along the west Patagonian margin over the entire Mesozoic Era, despite episodic events of tectonic erosion of coherent fragments.

Zircon Record of Subduction Evolution

Lazaro unit rocks (sample 24 from Angiboust et al., 2017; sample AL12 from Hervé and Fanning, 2002) exhibit a cluster of zircon ages of 178–157 Ma, including low-Th/U ratio overgrowths rimming older zircon crystals, such as 298–266 Ma cores (Fig. 8A; Hervé and Fanning, 2002; see also fig. 14 from Angiboust et al., 2017). Angiboust et al. (2017) interpreted these zircon rims as a result of a HT partial melting event that took place in a hot subduction setting at ca. 165 Ma (Figs. 8A and 9). By contrast, the Almagro HP-LT complex samples 39 and 47a (this work) and the quartz-rich mica schist AL16 from Hervé and Fanning (2002) from the Garnet Amphibolite unit have a wide range of ages that range from Early Jurassic to Early Cretaceous (Fig. 8B). The zircon age distribution can be classified into two groups (Fig. 8B). The first group comprises prismatic crystals with oscillatory zoning and ages of

Figure 7. Frequency and density distribution of U-Pb sensitive high-resolution ion microprobe (SHRIMP) zircon ages. (A) Pre-Triassic basement from east Patagonia, with compiled data from (1) Pankhurst et al. (2003); (2) Pankhurst et al. (2006); and (3) Moreira et al. (2013). DAI—Diego de Almagro Island; DM—Deseado Massif; SCM—Somun Cura Massif; TIMS—thermal ionization mass spectrometry. (B) Late Devonian to Early Triassic metasedimentary rocks from metamorphic complexes (MC) of southern Chile, compiled data from: (1) Hervé and Fanning (2001); (2) Hervé and Fanning (2002); (3) Hervé et al. (2003); (4) Augustsson et al. (2006); and (5) Sepúlveda et al. (2010). (C) Seno Arcabuz sample 48c from (1) present work. (D) Lazaro unit, compiled data from (1) Hervé and Fanning (2002) and (2) Angiboust et al. (2017). (E) Almagro high-pressure–low-temperature (HP-LT) complex Garnet Amphibolite unit (GA) samples 47a and 39 (present work) and compiled data from Hervé et al. (2003), and Blueschist unit (BS) sample 43 (present work). To facilitate comparison in all plots, vertical bands indicate comparable ages in all considered data. *N*—number of individual samples; *n*—zircon point ages. Schematic maps indicating the sample locations are shown at right. STA—Statherian; CA—Calymmian; EC—Ectasian; ST—Stenian; TO—Tonian; CR—Cryogenian; ED—Ediacaran; CM—Cambrian; O—Ordovician; S—Silurian; D—Devonian; C—Carboniferous; P—Permian; T—Triassic.

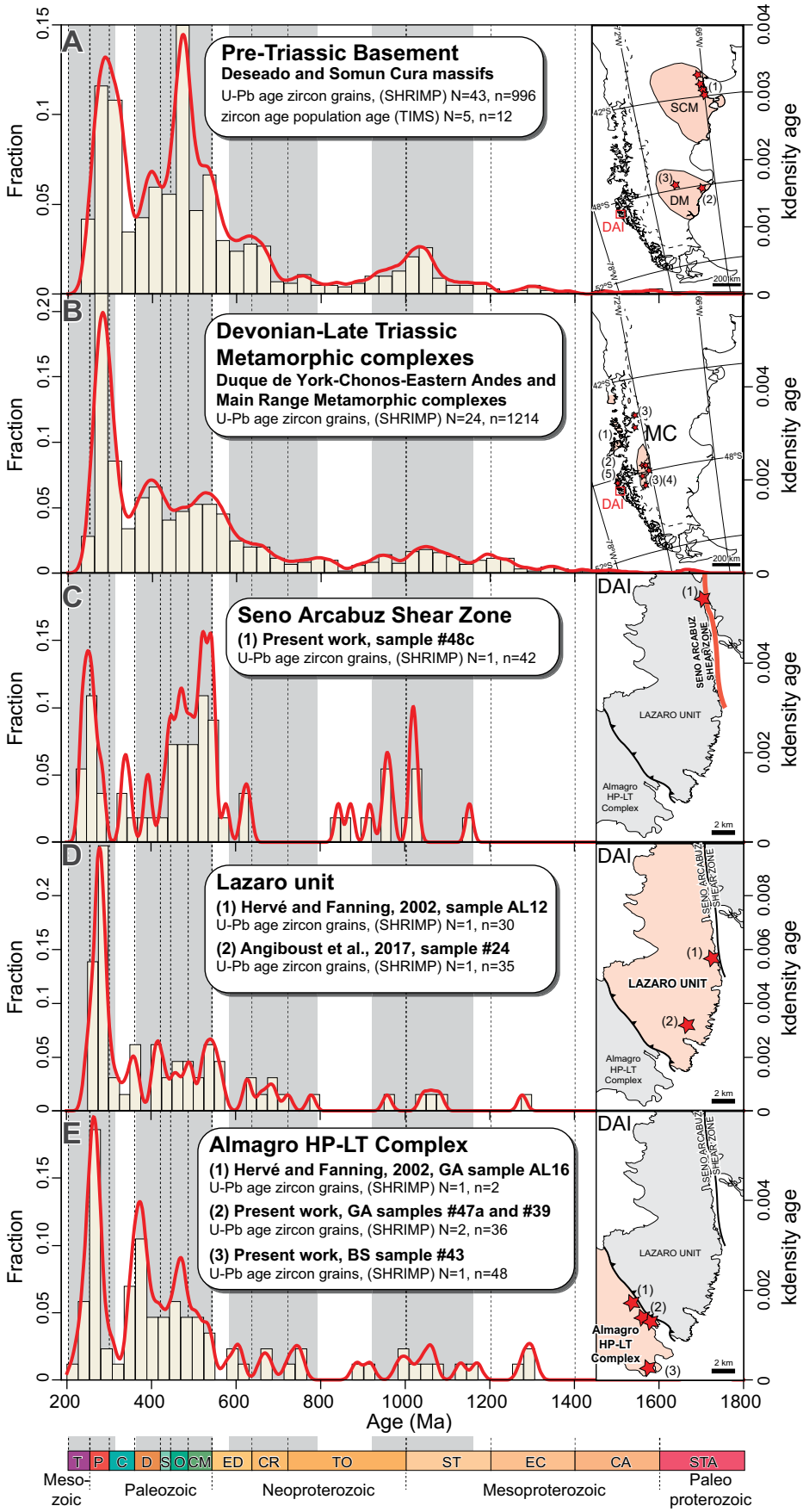

193–157 Ma (Figs. 5B and 5C; see also fig. 2A from Hervé and Fanning 2002). We consider this 193–157 Ma zircon population as detrital and related to the episodic silicic volcanism in Patagonia and Antarctic Peninsula that occurred from the Early to Late Jurassic (192–145 Ma; Fig. 8C; Pankhurst et al., 2000; Calderón et al., 2007; Riley et al., 2017). The erosion and dismantling of volcanic edifices favored the transport of these zircon crystals into basins. The sedimentary rocks of these basins were later subducted and affected by a HP event. Sample AL16 in Hervé and Fanning (2002) corresponds to a discrete siliceous layer intercalated in the sequence of metabasalts exposed in the Puerto de Almagro area (Fig. 1C). In our view, the zircon groups with ages of 183 ± 4 Ma (n = 7), 174 ± 2 Ma (n = 10), 166 ± 2 Ma (n = 26), and 157 ± 3 Ma (n = 5; Fig. 8B) that these authors report suggest that this layer may record a sequence of massive ignimbritic, ash-flow events

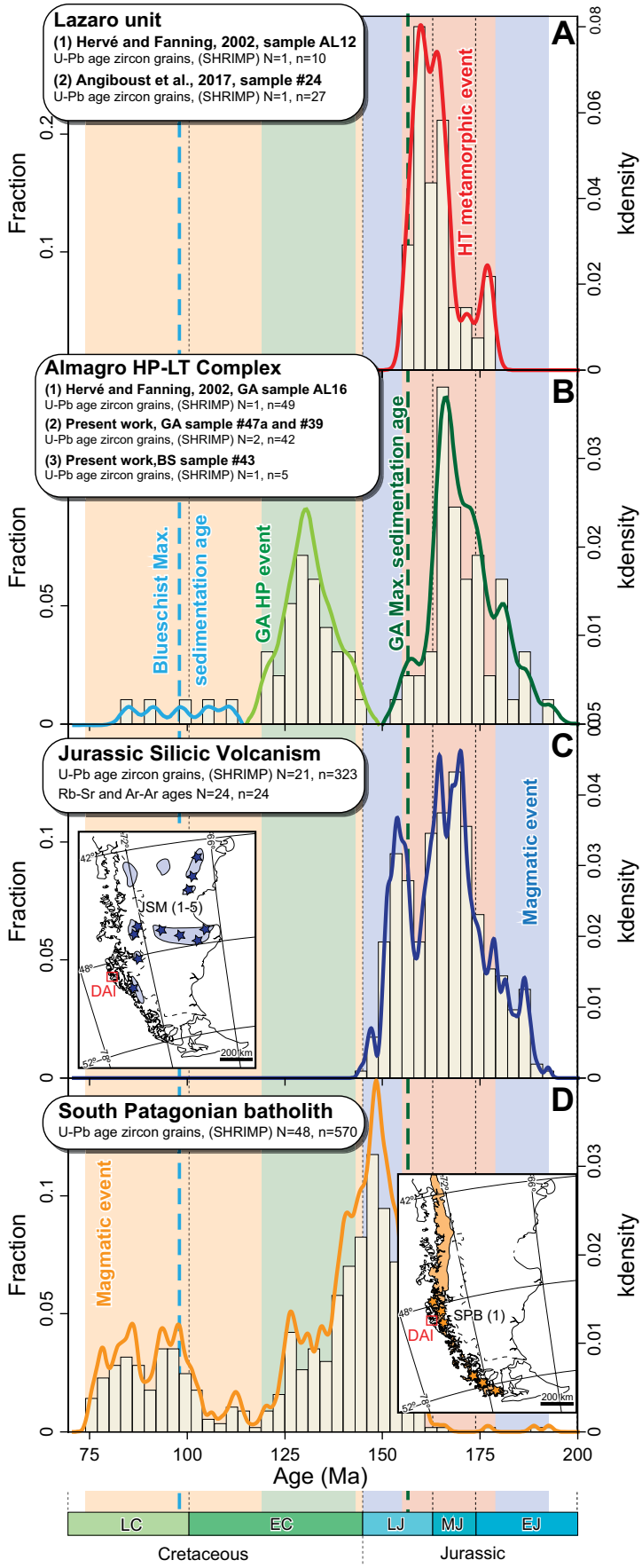

Figure 8. Summary of Mesozoic zircon data for the Diego de Almagro metamorphic complex. (A) Lazaro unit, compiled data from: (1) Hervé and Fanning (2002) and (2) Angiboust et al. (2017). HT—high temperature. (B) Almagro high-pressure–low-temperature (HP-LT) complex Garnet Amphibolite unit (GA) samples 47a and 39 and compiled data from Hervé and Fanning (2002), and Blueschist unit (BS) sample 43. HP—high pressure. (C) Frequency and density distribution of U-Pb ion microprobe and whole-rock ages of volcanic rocks from Jurassic silicic volcanism (JSM) event in Patagonia, compiled data from (1) Rapela and Pankhurst (1993); (2) Pankhurst et al. (1993); (3) Pankhurst and Rapela (1995); (4) Alric et al. (1996); and (5) Pankhurst et al. (2000). DAI—Diego de Almagro Island. (D) Frequency and density distribution of U-Pb sensitive high-resolution ion microprobe (SHRIMP) zircon ages from South Patagonian Batholith (SPB), with compiled data from Hervé et al. (2007). Schematic map indicates the sample locations. To facilitate comparison in all plots, vertical bands discriminate the metamorphic and magmatic events, as well as the maximum sedimentation ages. *N*—number of individual samples; *n*—zircon ages. LC—Late Cretaceous; EC—Early Cretaceous; LJ—Late Jurassic; MJ—Middle Jurassic; EJ—Early Jurassic.

deposited in the oceanic basin during an extensive volcanically active interval (e.g., Miller and Wark, 2008). The maximum sedimentation age can therefore be established at 157 ± 3 Ma for the Garnet Amphibolite unit (Fig. 8B).

The second zircon group is characterized by Early Cretaceous ages (144–120 Ma; Fig. 8B). Zircon domains of this age cluster are rims with low Th/U ratio (0.003–0.03) overgrowing older zircon grains, including a ca. 172 Ma core (Figs. 5A, 6B, and 6C). Thus, we consider the zircon rims formed on samples 39 and 47a as metamorphic in origin. These metamorphic zircon domains from the garnet amphibolite unit yield a weighted mean (errors reported at 2σ, n = 34) ^{208}Pb-corrected ^{206}Pb/^{238}U age of 131 ± 2 Ma (MSWD = 4.36) and ^{207}Pb/^{235}U age of 133 ± 2 Ma (MSWD = 0.05). This age range is ~10 m.y. older than the ca. 120 Ma amphibolite-facies overprint recorded in the Garnet Amphibolite unit (see Rb-Sr data in Hyppolito et al., 2016; Fig. 9A). We propose here that the metamorphic rims visible on zircon crystals from samples 39 and 47a record a stage of zircon growth during prograde metamorphic condi-

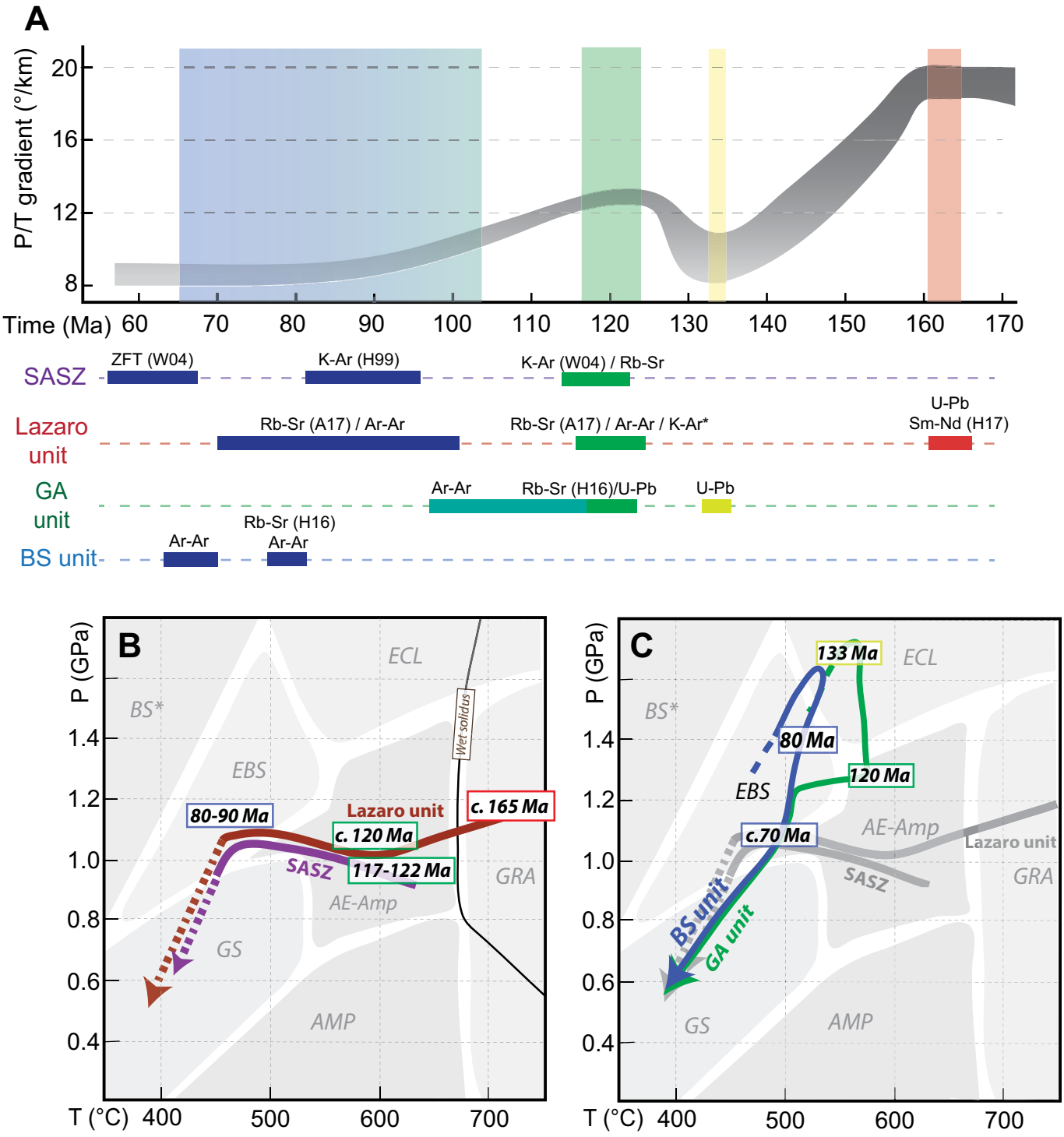

Figure 9. Summary of pressure-temperature-time (*P-T-t*) data. (A) Approximate evolution of the subduction thermal gradient from Early Jurassic to Late Cretaceous based on individual ig*P-T-t* estimates for the four units identified on Diego de Almagro Island. See also the summary of the geochronological results below for each unit. The K-Ar (W04) and zircon fission-track (ZFT) data are from Willner et al. (2004a). H16—age data from Hyppolito et al. (2016); A17—age data from Angiboust et al. (2017); H99—K-Ar data from Hervé et al. (1999). The thick, gray shaded line reflects an estimate of the uncertainty on the thermal gradient estimate. SASZ—Seno Arcabuz shear zone. (B–C) Summary of the proposed *P-T-t* paths for the Lazaro unit (Angiboust et al., 2017), the Seno Arcabuz shear zone (Data Repository Appendix DR1 [see text footnote 1]), and the Almagro high-pressure–low-temperature (HP-LT) Blueschist (BS) and Garnet Amphibolite (GA) units (Hyppolito et al., 2016). Note that all the *P-T* paths apparently converge toward the 1.0 GPa region (~35 km depth). ECL—Eclogite facies; BS*—Blueschist facies; EBS—Epidote Blueschist facies; GS—Greenschist facies; AE-Amp—Epidote Amphibolite facies; AMP—Amphibolite facies; GRA—Granulite facies.

tions (Fig. 9C). Prograde breakdown of ilmenite to rutile or titanite could represent a good candidate to explain the release of the Zr needed to form these overgrowths (e.g., Bingen et al., 2001). These new age results enable completion of the *P-T-t* path proposed by Hyppolito et al. (2016) for the garnet amphibolite unit, yielding an approximate residence time estimation of ~10 m.y. under HP metamorphic conditions (i.e., between 130 and 120 Ma; Fig. 9).

The Blueschist unit sample 43 exhibits some zircon grains with prismatic morphologies, oscillatory zoning, moderate Th/U ratios of 0.5–0.97, and the youngest U-Th-Pb ages from Diego de Almagro Island (110–90 Ma; Figs. 5D and 6D). These zircon grains are considered as detrital, possibly originating from the dismantling of the South Patagonian Batholith (emplaced between ca. 150 Ma and ca. 15 Ma; Hervé et al., 2007; Fig. 8D) or their associated volcanic products. These zircon grains were transported over large distances in the oceanic basin, followed by subduction and metamorphism under blueschist-facies conditions. The absence of detrital zircon crystals within the age range 150–115 Ma (Fig. 6D) could be related to the presence of a topographical barrier triggered by pluton emplacement and associated uplift (e.g., Willner, 2005) and/or result from surface uplift generated by tectonic accretion along the subduction interface (e.g., Willett et al., 2001). Hence, we provide a tentative estimate of the maximum sedimentation age at 97 ± 5 Ma for the Blueschist unit (Fig. 8D). The relatively young maximum sedimentation ages yielded by the Blueschist unit demonstrate that this unit was the last from the Diego de Almagro Island slice stack to enter the subduction channel.

Last, zircon age patterns for Garnet Amphibolite unit and Blueschist unit samples reveal a common origin for these two units, which is further supported by analogous lithological and geochemical affinities (Hyppolito et al., 2016). We propose that both units represent distinct segments from the same oceanic basin (the proto-Pacific ocean floor; e.g., Mpodozis and Forsythe, 1983). An approximate horizontal distance of ~2000 km between the Garnet Amphibolite unit and Blueschist unit locations can be estimated, considering a continuous, ~40 m.y. subduction and an average and constant ~5 cm/yr subduction rate. This statement confirms that the basal part of Diego de Almagro Island was formed by accretion of open-sea sediments during the Late Cretaceous.

Long-Lasting Record of Subduction History

Diego de Almagro Island represents a unique window onto the different structural levels of the Mesozoic paleo–accretionary wedge in Chilean Patagonia. As already recognized by Willner et al. (2004a), Diego de Almagro Island consists of several bodies that witnessed heterogeneous thermal histories. The recent work from Hyppolito et al. (2016) and Angiboust et al. (2017) combined with the new results presented here enable the reconstruction of individual *P-T-t* paths for the different elements that constitute Diego de Almagro Island (Table 1; Fig. 9). The earliest metamorphic event recorded on the island is preserved in the Lazaro unit, where seafloor material metamorphosed under HP-HT conditions was decoupled from the downgoing slab and accreted at a depth of ~45 km under a hot prograde subduction thermal regime (16–20°/km; Fig. 9; Angiboust et al., 2017). *P-T-t* reconstructions have shown that the Lazaro unit underwent a long-lasting stage of isobaric cooling along the hanging wall of the subduction interface (down to 8–10°/km; Fig. 9). The coeval, ca. 120 Ma amphibolite-facies imprint recorded by Seno Arcabuz Shear zone rocks, by the Lazaro unit, and by the garnet amphibolite unit (Willner et al., 2004a; Hyppolito et al., 2016; Table 1; Fig. 9A) indicates that the juxtaposition of each of these slices occurred ca. 120 Ma in the amphibolite facies. These findings confirm the importance of the 30–40 km depth range for juxtaposing tectonic slices from various depths prior to the onset of forced return flow across the forearc crust (e.g., Willner et al., 2005). The slight maximum pressure differences recorded by Seno Arcabuz shear zone and Lazaro slices for the amphibolitization stage suggest some complex interface-parallel tectonic transport processes in the 0.9–1.3 GPa range, which need further detailed investigations in order to be more precisely resolved (Figs. 9B and 9C).

Later, an upper-greenschist-facies to epidote-blueschist-facies metamorphic event affected these three units to variable extents, as shown by the heterogeneous development of thin, phengite-rich rims around coarse-grained amphibolite-facies white mica crystals (Angiboust et al., 2017; Willner et al., 2004a; Data Repository Appendix DR1 [see footnote 1]). This process led to (1) the tectonic reworking of primary kinematic indicators, blurred by this younger and pervasive event, and (2) partial resetting of the isotopic signature, as visible, for example, in the Ar-Ar and Rb-Sr age data along the Puerto shear zone, at the base of the Lazaro

TABLE 1. SUMMARY OF SAMPLES USED FOR GEOCHRONOLOGICAL WORK

Sample	Unit		Rock name	Main paragenesis (+Qz)	Method	Maximum sedimentation age (Ma)	Metamorphic ages (Ma)
48b	SASZ		Mafic schist	Hbl-Ep-Ms-Bt-Pl-Ilm	Multimineral Rb-Sr		117 ± 2.6 (amphibolite-facies shearing)
48c			Mafic schist	Hbl-Ep-Ms-Bt-Pl-Ilm	U-Th-Pb Zrn (SHRIMP)	ca. 255	No Mesozoic Zrn
24	Lazaro unit	LU	Paragneiss	Ms-Grt-Chl-Pl-Ttn	Ar-Ar (WM)	ca. 251 (1)	100–130 (cooling of Lazaro HP granulites)
29a		PSZ	Mica schist	Ms-Chl-Ab-Ttn	Ar-Ar (WM)		73 ± 3 (retrograde shearing)
47a	Almagro HP-LT complex	GA	Mica schist	Phg-Grt-Hbl-Ab-Ttn	U-Th-Pb Zrn (SHRIMP)	ca. 157 (2), ca. 175 (3)	130–135 (peak burial metamorphism)
39			Mica schist	Phg-Grt-Hbl-Ab-Ttn	U-Th-Pb Zrn (SHRIMP)	ca. 180 (3)	125–135 (peak burial metamorphism)
39c			Mica schist	Ms-Grt-Hbl-Ab-Ttn	Ar-Ar (WM)		103 ± 5 (cooling of GA unit)
43		BS	Mica schist	Gln-Ep-Chl-Ab-Phg	U-Th-Pb Zrn (SHRIMP)	ca. 97	<10 µm Zrn rims (too thin for SHRIMP analysis)
18a			Mafic tuff	Gln-Ep-Chl-Ab-Phg	Ar-Ar (WM)		80 ± 2 (peak burial metamorphism)
223j			Mica schist	Ms-Grt-Chl-Ab-Ttn	Ar-Ar (WM)		67 ± 4 (peak burial metamorphism)

Note: Data from (1) Angiboust et al. (2017), (2) Hervé and Fanning (2002), (3) present work. HP-LT—high-pressure–low-temperature; SASZ—Seno Arcabuz shear zone; LU—Lazaro unit; PSZ—Puerto shear zone; GA—Garnet Amphibolite unit; BS—Blueschist unit. SHRIMP—sensitive high-resolution ion microprobe; WM—white mica; Zrn—zircon; HP—high pressure. Mineral abbreviations follow the nomenclature of Whitney and Evans (2010).

unit (Figs. 2A, 4, and 9A). While the timing of the ca. 80 Ma blueschist-facies event has been precisely constrained based on consistent Rb-Sr and Ar-Ar age data (Hyppolito et al., 2016; this work), the apparent Ar-Ar age span between 110 Ma and 90 Ma in Lazaro unit and Garnet Amphibolite unit rocks is rather believed to reflect partial age resetting during incomplete re-equilibration of the ca. 120 Ma signal during the ca. 80 Ma deformation event (Table 1; Fig. 9). The Ar-Ar ages younger than ca. 80 Ma (29a and 223j) may also be explained by the partial reopening of the blueschist-facies fabric during a younger deformation event. In the Puerto shear zone, this post–80 Ma event may correspond to the deformation that triggered the juxtaposition and the underplating of the Blueschist unit below the Garnet Amphibolite unit near ~40 km depth, some millions of years after peak burial conditions at ~60 km depth and ca. 80 Ma (Fig. 10).

Our widely distributed age data reveal that the Diego de Almagro Island nappe stack fossilized the evolution of subduction interface deformation between 165 Ma and 70 Ma, i.e., over nearly ~100 m.y. (for similar observations on Paleozoic rocks in central Chile, see Willner et al., 2005). Natural occurrences of paleo–subduction zones with such a long-term metamorphic record are rare and include HP metamorphic complexes in Cuba (e.g., Lázaro et al., 2009; Despaigne-Díaz et al., 2016), Dominican Republic (Krebs et al., 2008), and California (e.g., Platt, 1986; Grove et al., 2008; Ducea et al., 2009; Wakabayashi, 2015). We interpret the discrete deformation-recrystallization pulses identified in our new geochronological data as evidence for transient episodes of underplating that led to the construction of Diego de Almagro Island as it is now visible in the field. The finding of the oldest metamorphic ages in the core of the Lazaro unit (ca. 165 Ma) and the youngest in the southwestermost end of Diego de Almagro Island ("Cabo Jorge"; point 223 on Fig. 1B; ca. 65 Ma) conforms with the idea that progressive down-stepping of plate interface deformation with ongoing accretionary processes is a common process in long-lived subduction zones (Fig. 10; Platt, 1986; Kimura et al., 1996; Glodny et al., 2005; Willner et al., 2005; Angiboust et al., 2014; Wakabayashi, 2015). This sequence of discrete accretion events is confirmed by the progressively younger maximum sedimentation ages observed from the Seno Arcabuz shear zone and Lazaro units (255–250 Ma) to the Almagro HP-LT complex Garnet Amphibolite unit (ca. 157 Ma) and lowermost Blueschist unit (ca. 97 Ma). The metamorphic history of Diego de Almagro Island is reminiscent of the long-term tectonic and thermal evolution reported for Catalina Island in the Franciscan complex in California, where coeval underplating and subduction thermal gradient cooling have been proposed (e.g., Grove et al., 2008, and references therein). This observation suggests that such long-term dynamics in the 35–40 km depth region may be the rule in most subduction zones worldwide (for such example in the Cascades region, see Calvert et al., 2011). Out-of-sequence tectonic reactivation of former thrust contacts during exhumation may have partially reset geochronological markers (as shown by relatively young Ar-Ar ages along the Puerto shear zone; Fig. 9A) but did not modify the overall deep duplex architecture remarkably recorded on Diego de Almagro Island.

Seno Arcabuz Shear Zone Deformation and Exhumation of Diego de Almagro Island

Understanding the evolution and the geological meaning of the Seno Arcabuz shear zone is critical because this first-order structural element may represent the former plate boundary prior to accretion of the Lazaro unit to the

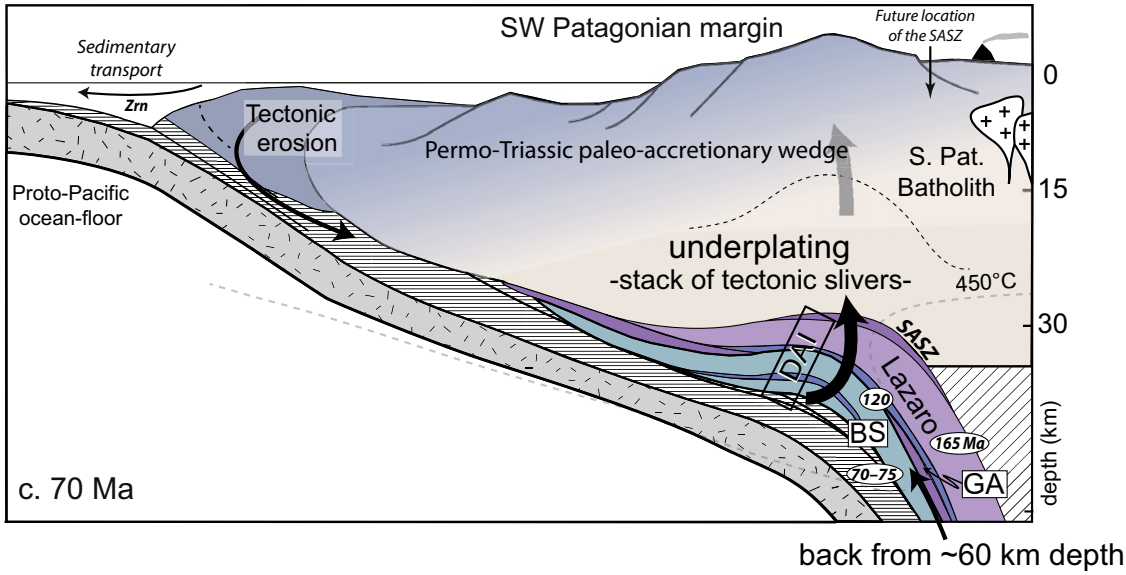

Figure 10. Tectonic sketch showing the inferred architecture of the deep accretionary wedge in the basal accretion region and the location of Diego de Almagro Island (DAI) at ca. 70 Ma, after underplating of the Blueschist unit exhumed in a subduction channel from greater depths. The horizontally ruled material along the plate interface represents the sediment-rich subduction channel. Note that the Permian–Triassic Madre de Dios accretionary complex composes a large part of the forearc crust. Seno Arcabuz shear zone (SASZ) and Lazaro units are colored in purpled and derive from the tectonic erosion of the Permian–Triassic wedge, while Garnet Amphibolite unit (GA) and Blueschist unit (BS) represent accreted material from the Mesozoic proto-Pacific ocean floor. The upward arrows represent the forced return flow of basally accreted rocks traveling through the forearc. Our results do not permit discrimination regarding whether the sliver corresponding to the Seno Arcabuz shear zone was accreted before or after the Lazaro unit. Zrn—zircon.

Gondwana margin. The zircon population signatures of Seno Arcabuz shear zone and Lazaro unit samples suggest that both units formed by tectonic erosion at the trench of fragments of the Permian–Triassic Madre de Dios accretionary complex, followed by underplating at 35–40 km depth (Figs. 9 and 10; Data Repository Appendix DR3 [see footnote 1]; Angiboust et al., 2017). Prograde actinolite inclusions are found in hornblende from Seno Arcabuz shear zone samples (Data Repository Appendix DR1 [see footnote 1]) but are absent from Lazaro unit amphibolites due to a higher metamorphic degree (Angiboust et al., 2017). In addition, peritectic garnet crystals that are widespread in the Lazaro unit have not been observed as cores in Seno Arcabuz shear zone samples. These two points suggest that the rocks forming the Seno Arcabuz shear zone represent a separate sliver (on the hanging wall of the Lazaro unit) derived from the Madre de Dios accretionary complex (Fig. 10). Microstructural observations combined with a Rb-Sr deformation age on sample 48b indicate that the amphibolite-facies deformation responsible for the juxtaposition with the underlying Lazaro unit occurred at around 117 Ma under a pressure of ~0.9 GPa and in the temperature range 600–640 °C (Figs. 3 and 10; Data Repository Appendix DR1 [see footnote 1]). The observation of a discrete and static HP-LT overprint over this mylonitic fabric suggests that the HT sinistral strike-slip deformation apparently ended along the Seno Arcabuz shear zone in the Late Cretaceous between ca. 117 Ma and ca. 65 Ma (see zircon fission-track ages of Willner et al., 2004a; Fig. 9A). We therefore hypothesize that the major part of Seno Arcabuz shear zone strike-slip deformation was related to oblique convergence and deformation partitioning during the Early Cretaceous subduction event. A younger white mica K-Ar age of 89 ± 8 Ma reported by Hervé et al. (1999; see also Olivares et al., 2003) may reflect partial recrystallization along the Seno Arcabuz shear zone during the Late Cretaceous associated with ongoing underplating in the basal accretion site under HP-LT conditions (Fig. 9).

Zircon and apatite fission-track ages given by Olivares et al. (2003) and Willner et al. (2004a) indicate that Seno Arcabuz shear zone rocks reached subsurface conditions during the Eocene. Some younger and cooler deformation is required to explain the present-day juxtaposition of Seno Arcabuz shear zone rocks at the same level as the adjacent Permian–Triassic LP-LT Madre de Dios accretionary complex. Since fault zones generally narrow with decreasing temperature, the missing structure probably lies in the Seno Arcabuz shear zone bay and is actually hardly visible on the shore (see Olivares et al., 2003; Fig. 1C). Further field investigations are needed to identify the structure that enabled the exhumation of the Seno Arcabuz shear zone from ~35 km depth to the subsurface. Given the similarity between exhumation paths for the Seno Arcabuz shear zone, the Lazaro unit, and Garnet Amphibolite unit (all these units exhibit, for instance, the same type of thin phengite overgrowths around muscovite crystals; see, e.g., Willner et al., 2004a; Data Repository Appendix DR1 [see footnote 1]), it is likely that the entire Diego de Almagro Island nappe stack was exhumed along this hidden structure (Fig. 10). Normal-faulting displacement along this structure also enabled the apparent juxtaposition of the South Patagonian Batholith together with the Diego de Almagro Island nappe stack. We stress that the depth (~35 km) of the processes recorded on Diego de Almagro Island during amphibolitization at ca. 120 Ma is more than four times greater than the inferred emplacement depth for the granitoids from the South Patagonian Batholith (~7 km depth; e.g., Parada et al., 2007, and references therein). In other words, a >25 km section of (accreted) material was removed above the Diego de Almagro Island slice stack between the mid-Cretaceous and late Eocene to enable its juxtaposition with the adjacent South Patagonian Batholith (Fig. 1). Vertical exhumation of the Diego de Almagro Island nappe stack through the forearc crust (e.g., Platt, 1986; Willner, 2005) implies that a very broad (>100-km-wide) Permian–Triassic wedge was present in a forearc position until the early Cenozoic (Fig. 10). This setting recalls the structure proposed by Willner (2005) for the Western series in central Chile, where such a thick Paleozoic wedge has been identified. The late exhumation of the Diego de Almagro slice stack, characterized by a massive greenschist-facies overprint and a crenulation cleavage (Willner et al., 2004a; Richter et al., 2007; Hyppolito et al., 2016), suggests a sluggish uplift rate during the crossing of the forearc crust, probably associated with ongoing underplating of younger units in the basal accretion site (Fig. 10).

CONCLUSIONS

Diego de Almagro Island represents an exhumed section composed of four tectonic slivers from the basal accretion region. Extensive petrological, geochemical, and geochronological investigations have led to the following conclusions:

(1) The four tectono-metamorphic units identified were successively accreted in the 35–40 km depth range at the base of a huge accretionary prism over a nearly 100 m.y. interval, beginning with HP granulite-facies metamorphism at ca. 165 Ma and terminating with an epidote blueschist event at ca. 80 Ma. Each shear zone separating the different slices can be viewed as a transient plate interface contact that was used until episodic down-stepping of the main deformation front and associated underplating of a new slice occurred. Our observations, which are similar to the mechanisms and the overall architecture described for Catalina Island in the Franciscan complex, shed light on a unique, large-scale window into the physical nature of the southern Chilean subduction interface region near the base of the seismogenic zone.

(2) Despite heterogeneous maximum burial depths (in the range of 40–60 km), the elements of the slice stack document the long-term evolution of the subduction thermal gradient from ~20°/km in the Middle Jurassic down to ~8°/km in the Late Cretaceous. The Lazaro unit records protracted metamorphic evolution of more than ~90 m.y.

(3) The provenance of the rocks now forming the island remained constant over the entire Mesozoic Era: All the units exhibit a zircon distribution signature very similar to the one from a Permian–Triassic paleo–accretionary wedge exposed in the forearc buttress. Evidence for tectonic erosion of this older wedge is observed in the two uppermost tectonic slivers (Seno Arcabuz shear zone and Lazaro unit), while the younger, lowermost units (Almagro HP-LT complex Garnet Amphibolite and Blueschist units) derive from the proto-Pacific ocean floor and exhibit younger zircon maximum sedimentation ages (up to ca. 97 Ma). The structure and mechanisms described on Diego de Almagro Island can be viewed as a representative, fossilized image of the deformation and the long-term thermal evolution of the southern Chilean forearc. These results will also shed light on the structure of the deep segments of accretionary wedges studied by geophysical methods and improve our understanding of crustal recycling along convergent margins through geologic time.

ACKNOWLEDGMENTS

This project was funded through a Deutsche Forschungsgemeinschaft (DFG) project to Angiboust (AN1113-1), by an IDEX research chair to Angiboust (16C538), and by the São Paulo Research Foundation (FAPESP; 2004/10203-7, 2012/01191-1), and support for analytical costs at the Centro de Instrumentación Científica (CIC) was provided by the University of Granada. A. Garcia-Casco is warmly thanked for insightful discussions. The constructive and insightful reviews from A. Willner, J. Berger, and C. Allen helped to improve this manuscript. Hyppolito acknowledges grant 2014/23422-0 (FAPESP) for a postdoctoral fellowship. This is IBERSIMS publication 47 and Institut de Physique du Globe de Paris (IPGP) contribution 3920.

REFERENCES CITED

Agard, P., Yamato, P., Jolivet, L., and Burov, E., 2009, Exhumation of oceanic blueschists and eclogites in subduction zones: Timing and mechanisms: Earth-Science Reviews, v. 92, no. 1-2, p. 53–79, https://doi.org/10.1016/j.earscirev.2008.11.002.

Alric, V.I., Haller, M.J., Féraud, G., Beretrand, H., and Zubia, M., 1996, Cronología ^{40}Ar-^{39}Ar del volcanismo jurásico de la Patagonia extraandina, *in* XIII Congreso Geológico Argentino y III Congreso Exploracion de Hidrocarburos: Buenos Aires, Instituto Argentino del Petroleo y del Gas, p. 243–250.

Angiboust, S., Agard, P., Jolivet, L., and Beyssac, O., 2009, The Zermatt-Saas ophiolite: The largest (60-km wide) and deepest (c. 70–80 km) continuous slice of oceanic lithosphere detached from a subduction zone?: Terra Nova, v. 21, no. 3, p. 171–180, https://doi.org/10.1111/j.1365-3121.2009.00870.x.

Angiboust, S., Glodny, J., Oncken, O., and Chopin, C., 2014, In search of transient subduction interfaces in the Dent Blanche–Sesia tectonic system (W. Alps): Lithos, v. 205, p. 298–321, https://doi.org/10.1016/j.lithos.2014.07.001.

Angiboust, S., Agard, P., Glodny, J., Omrani, J., and Oncken, O., 2016, Zagros blueschists: Episodic underplating and long-lived cooling of a subduction zone: Earth and Planetary Science Letters, v. 443, p. 48–58, https://doi.org/10.1016/j.epsl.2016.03.017.

Angiboust, S., Hyppolito, T., Glodny, J., Cambeses, A., Garcia-Casco, A., Calderón, M., and Juliani, C., 2017, Hot subduction in the Middle Jurassic and partial melting of oceanic crust in Chilean Patagonia: Gondwana Research, v. 42, p. 104–125, https://doi.org/10.1016/j.gr.2016.10.007.

Augustsson, C., Münker, C., Bahlburg, H., and Fanning, C.M., 2006, Provenance of late Palaeozoic metasediments of the SW South American Gondwana margin: A combined U-Pb and Hf-isotope study of single detrital zircons: Journal of the Geological Society[London], v. 163, p. 983–995, https://doi.org/10.1144/0016-76492005-149.

Bingen, B., Austrheim, H., and Whitehouse, M., 2001, Ilmenite as a source for zirconium during high-grade metamorphism? Textural evidence from the Caledonides of western Norway and implications for zircon geochronology: Journal of Petrology, v. 42, no. 2, p. 355–375, https://doi.org/10.1093/petrology/42.2.355.

Black, L.P., Kamo, S.L., Allen, C.M., Aleinikoff, J.A., Davis, D.W., Korsch, J.R., and Foudolis, C., 2003, TEMORA 1: A new zircon standard for Phanerozoic U-Pb geochronology: Chemical Geology, v. 200, p. 155–170, https://doi.org/10.1016/S0009-2541(03)00165-7.

Calderón, M., Fildani, A., Hervé, F., Fanning, C.M., Weislogel, A., and Cordani, U., 2007, Late Jurassic bimodal magmatism in the northern sea-floor remnant of the Rocas Verdes basin, southern Patagonian Andes: Journal of the Geological Society [London], v. 164, no. 5, p. 1011–1022, https://doi.org/10.1144/0016-76492006-102.

Calderón, M., Prades, C.F., Hervé, F., Avendaño, V., Fanning, C.M., Massonne, H.J., Theye, T., and Simonetti, A., 2013, Petrological vestiges of the Late Jurassic–Early Cretaceous transition from rift to back-arc basin in southernmost Chile: New age and geochemical data from the Capitán Aracena, Carlos III, and Tortuga ophiolitic complexes: Geochemical Journal, v. 47, no. 2, p. 201–217, https://doi.org/10.2343/geochemj.2.0235.

Calderón, M., Hervé, F., Fuentes, F., Fosdick, J.C., Sepúlveda, F., and Galaz, G., 2016, Tectonic evolution of Paleozoic and Mesozoic Andean metamorphic complexes and the Rocas Verdes ophiolites in southern Patagonia, *in* Ghiglione, M.C., ed., Geodynamic Evolution of the Southernmost Andes: Springer, Earth System Sciences, p. 7–36, https://doi.org/10.1007/978-3-319-39727-6_2.

Calvert, A.J., Preston, L.A., and Farahbod, A.M., 2011, Sedimentary underplating at the Cascadia mantle-wedge corner revealed by seismic imaging: Nature Geoscience, v. 4, no. 8, p. 545, https://doi.org/10.1038/ngeo1195.

Castillo, P., Fanning, C.M., Hervé, F., and Lacassie, J.P., 2016, Characterisation and tracing of Permian magmatism in the south-western segment of the Gondwanan margin; U-Pb age, Lu-Hf and O isotopic compositions of detrital zircons from metasedimentary complexes of northern Antarctic Peninsula and western Patagonia: Gondwana Research, v. 36, p. 1–13, https://doi.org/10.1016/j.gr.2015.07.014.

Charrier, R., Pinto, L., and Rodríguez, M.P., 2007, Tectonostratigraphic evolution of the Andean Orogen in Chile, *in* Moreno, T., and Gibbons, W., eds., The Geology of Chile: Geological Society, London, Special Publication, p. 21–114.

Claoué-Long, J., Compston, W., Roberts, J., and Fanning, C.M., 1995, Two Carboniferous ages: A comparison of SHRIMP zircon dating with conventional zircon ages and ^{40}Ar/^{39}Ar analysis, *in* Berggren, W.A., Kent, D.V., Aubry, M.P., and Hardenbol, J., eds., Geochronology, Time Scales & Stratigraphic Correlation: Society for Sedimentary Geology (SEPM) Special Publication 54, p. 3–21, https://doi.org/10.2110/pec.95.04.0003.

Cloos, M., and Shreve, R.L., 1988, Subduction-channel model of prism accretion, mélange formation, sediment subduction, and subduction erosion at convergent plate margins: 1. Background and description: Pure and Applied Geophysics, v. 128, no. 3-4, p. 455–500, https://doi.org/10.1007/BF00874548.

Despaigne-Díaz, A.I., García-Casco, A., Govea, D.C., Jourdan, F., Wilde, S.A., and Trujillo, G.M., 2016, Twenty-five million years of subduction-accretion-exhumation during the Late Cretaceous–Tertiary in the northwestern Caribbean: The Trinidad Dome, Escambray complex, central Cuba: American Journal of Science, v. 316, no. 3, p. 203–240, https://doi.org/10.2475/03.2016.01.

Ducea, M.N., Kidder, S., Chesley, J.T., and Saleeby, J.B., 2009, Tectonic underplating of trench sediments beneath magmatic arcs: The central California example: International Geology Review, v. 51, no. 1, p. 1–26, https://doi.org/10.1080/00206810802602767.

Ernst, W.G., and Dal Piaz, G.V., 1978, Mineral parageneses of eclogitic rocks and related mafic schists of the Piemonte ophiolite nappe, BreuiléSt. Jacques area, Italian western Alps: The American Mineralogist, v. 63, no. 7-8, p. 621–640.

Faure, G., 1986, Principles of Isotope Geology: New York, Wiley, 615 p.

Forsythe, R., and Mpodozis, C., 1983, Geología del Basamento Pre-Jurásico Superior en el Archipiélago Madre de Dios, Magallanes, Chile: Servicio Nacional de Geología y Minería (Chile) Boletín Numéro 39, 63 p.

Glodny, J., Lohrmann, J., Echtler, H., Gräfe, K., Seifert, W., Collao, S., and Figueroa, O., 2005, Internal dynamics of a paleoaccretionary wedge: Insights from combined isotope tectonochronology and sandbox modelling of the south-central Chilean forearc: Earth and Planetary Science Letters, v. 231, no. 1-2, p. 23–39, https://doi.org/10.1016/j.epsl.2004.12.014.

Glodny, J., Kühn, A., and Austrheim, H., 2008, Diffusion versus recrystallization processes in Rb-Sr geochronology: Isotopic relics in eclogite facies rocks, Western Gneiss Region, Norway: Geochimica et Cosmochimica Acta, v. 72, no. 2, p. 506–525, https://doi.org/10.1016/j.gca.2007.10.021.

Grove, M., Bebout, G.E., Jacobson, C.E., Barth, A.P., Kimbrough, D.L., King, R.L., Zou, H., Lovera, O.M., Mahoney, B.J., and Gehrels, G.E., 2008, The Catalina Schist: Evidence for middle Cretaceous subduction erosion of southwestern North America, in Draut, A.E., Clift, P.D., and Scholl, D.W., eds., Formation and Applications of the Sedimentary Record in Arc Collision Zones: Geological Society of America Special Paper 436, p. 335–361, https://doi.org/10.1130/2008.2436(15).

Hervé, F., 1988, Late Paleozoic subduction and accretion in southern Chile: Episodes, v. 11, no. 3, p. 183–188.

Hervé, F., and Fanning, C.M., 2001, Late Triassic detrital zircons in metaturbidites of the Chonos metamorphic complex, southern Chile: Revista Geológica de Chile, v. 28, p. 91–104, https://doi.org/10.4067/S0716-02082001000100005.

Hervé, F., and Fanning, C.M., 2002, Early Cretaceous subduction of continental crust at the Diego de Almagro archipelago, southern Chile: Episodes, v. 26, p. 285–289.

Hervé, F., Prior, D., López, G., Ramos, V., Rapalini, A., Thomson, S., and Fanning, M., 1999, Mesozoic blueschists from Diego de Almagro, southern Chile, *in* South American Symposium on Isotope Geology, Actas, Volume 2: Cordoba, Argentina, Subsecretaría de Minería de la Nación, p. 318–321.

Hervé, F., Fanning, C.M., and Pankhurst, R.J., 2003, Detrital zircon age patterns and provenance in the metamorphic complexes of southern Chile: Journal of South American Earth Sciences, v. 16, p. 107–123, https://doi.org/10.1016/S0895-9811(03)00022-1.

Hervé, F., Pankhurst, R.J., Fanning, C.M., Calderón, M., and Yaxley, G.M., 2007, The South Patagonian Batholith: 150 my of granite magmatism on a plate margin: Lithos, v. 97, no. 3-4, p. 373–394, https://doi.org/10.1016/j.lithos.2007.01.007.

Hilairet, N., and Reynard, B., 2009, Stability and dynamics of serpentinite layer in subduction zone: Tectonophysics, v. 465, no. 1-2, p. 24–29, https://doi.org/10.1016/j.tecto.2008.10.005.

Hyppolito, T.N., 2010, Termobarometria, Evolução Tectono-Metamórfica, e Geoquímica de Xistos Azuis, Rochas Eclogíticas e Litotipos Associados da Ilha Diego de Almagro, Patagônia Chilena [M.S. thesis]: São Paulo, Brazil, Universidade de São Paulo, 173 p.

Hyppolito, T., García-Casco, A., Juliani, C., Meira, V.T., and Hall, C., 2014, Late Paleozoic onset of subduction and exhumation at the western margin of Gondwana (Chilenia terrane): Counterclockwise *P-T* paths and timing of metamorphism of deep-seated garnet–mica schist and amphibolite of Punta Sirena, Coastal accretionary complex, central Chile (34 S): Lithos, v. 206–207, p. 409–434, https://doi.org/10.1016/j.lithos.2014.07.023.

Hyppolito, T., Angiboust, S., Juliani, C., Glodny, J., Garcia-Casco, A., Calderón, M., and Chopin, C., 2016, Eclogite-, amphibolite- and blueschist-facies rocks from Diego de Almagro Island (Patagonia): Episodic accretion and thermal evolution of the Chilean subduction interface during the Cretaceous: Lithos, v. 264, p. 422–440, https://doi.org/10.1016/j.lithos.2016.09.001.

Inger, S., and Cliff, R.A., 1994, Timing of metamorphism in the Tauern Window, eastern Alps: Rb-Sr ages and fabric formation: Journal of Metamorphic Geology, v. 12, no. 5, p. 695–707, https://doi.org/10.1111/j.1525-1314.1994.tb00052.x.

Kato, T.T., 1985, Pre-Andean orogenesis in the Coast Ranges of central Chile: Geological Society of America Bulletin, v. 96, no. 7, p. 918–924, https://doi.org/10.1130/0016-7606(1985)96<918:POITCR>2.0.CO;2.

Kato, T.T., Sharp, W.D., and Godoy, E., 2008, Inception of a Devonian subduction zone along the southwestern Gondwana margin: ^{40}Ar-^{39}Ar dating of eclogite-amphibolite assemblages in blueschist boulders from the Coastal Range of Chile (41°S): Canadian Journal of Earth Sciences, v. 45, no. 3, p. 337–351, https://doi.org/10.1139/E08-006.

Kimura, G., Maruyama, S., Isozaki, Y., and Terabayashi, M., 1996, Well-preserved underplating structure of the jadeitized Franciscan complex, Pacheco Pass, California: Geology, v. 24, no. 1, p. 75–78, https://doi.org/10.1130/0091-7613(1996)024<0075:WPUSOT>2.3.CO;2.

Konstantinovskaya, E., and Malavieille, J., 2011, Thrust wedges with décollement levels and syntectonic erosion: A view from analog models: Tectonophysics, v. 502, no. 3-4, p. 336–350, https://doi.org/10.1016/j.tecto.2011.01.020.

Koppers, A.A., 2002, ArArCALC—Software for ^{40}Ar/^{39}Ar age calculations: Computers & Geosciences, v. 28, no. 5, p. 605–619, https://doi.org/10.1016/S0098-3004(01)00095-4.

Krebs, M., Maresch, W.V., Schertl, H.P., Münker, C., Baumann, A., Draper, G., Idleman, B., and Trapp, E., 2008, The dynamics of intra-oceanic subduction zones: A direct comparison between fossil petrological evidence (Rio San Juan complex, Dominican Republic) and numerical simulation: Lithos, v. 103, no. 1-2, p. 106–137, https://doi.org/10.1016/j.lithos.2007.09.003.

Kukowski, N., and Oncken, O., 2006, Subduction erosion—The "normal" mode of fore-arc material transfer along

the Chilean margin?, *in* Oncken, O., Chong, G., Franz, G., Giese, P., Götze, H.J., Ramos, V.A., Strecker, M.R., and Wigger, P., eds., The Andes: Berlin, Springer, p. 217–236, https://doi.org/10.1007/978-3-540-48684-8_10.

Lázaro, C., García-Casco, A., Rojas Agramonte, Y., Kröner, A., Neubauer, F., and Iturralde-Vinent, M., 2009, Fifty-five-million-year history of oceanic subduction and exhumation at the northern edge of the Caribbean plate (Sierra del Convento mélange, Cuba): Journal of Metamorphic Geology, v. 27, no. 1, p. 19–40, https://doi.org/10.1111/j.1525-1314.2008.00800.x.

Ludwig, K., 2009a, Isoplot: A User's Manual Rev. 12 Apr, 2012: Berkeley Geochronology Center Special Publication 1a, p. 5–110.

Ludwig, K., 2009b, SQUID 2 (Rev. 2.50), A User's Manual: Berkeley Geochronology Center Special Publication 5, 110 p.

Maluski, H., and Monié, P., 1988, ^{40}Ar-^{39}Ar laser probe multi-dating inside single biotites of a Variscan orthogneiss (Pinet, Massif Central, France): Chemical Geology–Isotope Geoscience Section, v. 73, no. 3, p. 245–263, https://doi.org/10.1016/0168-9622(88)90005-X.

Maruyama, S., Liou, J.G., and Terabayashi, M., 1996, Blueschists and eclogites of the world and their exhumation: International Geology Review, v. 38, no. 6, p. 485–594, https://doi.org/10.1080/00206819709465347.

McDougall, I., and Harrison, T.M., 1999, Geochronology and Thermochronology by the ^{40}Ar/^{39}Ar Method: Oxford, UK, Oxford University Press, 269 p.

Megrue, G.H., 1973, Spatial distribution of ^{40}Ar/^{39}Ar ages in lunar breccia 14301: Journal of Geophysical Research, v. 78, no. 17, p. 3216–3221, https://doi.org/10.1029/JB078i017p03216.

Miller, C.F., and Wark, D.A., 2008, Supervolcanoes and their explosive supereruptions: Elements, v. 4, no. 1, p. 11–15, https://doi.org/10.2113/GSELEMENTS.4.1.11.

Min, K., Mundil, R., Renne, P.R., and Ludwig, K.R., 2000, A test for systematic errors in ^{40}Ar/^{39}Ar geochronology through comparison with U/Pb analysis of a 1.1-Ga rhyolite: Geochimica et Cosmochimica Acta, v. 64, no. 1, p. 73–98, https://doi.org/10.1016/S0016-7037(99)00204-5.

Moreira, P., Fernández, R., Hervé, F., Fanning, M., and Schalamuk, I.A., 2013, Detrital zircons U-Pb SHRIMP ages and provenance of La Modesta Formation, Patagonia Argentina: Journal of South American Earth Sciences, v. 47, p. 32–46, https://doi.org/10.1016/j.jsames.2013.05.010.

Mpodozis, C., and Forsythe, R., 1983, Stratigraphy and geochemistry of accreted fragments of the ancestral Pacific floor in southern South America: Palaeogeography, Palaeoclimatology, Palaeoecology, v. 41, no. 1-2, p. 103–124, https://doi.org/10.1016/0031-0182(83)90079-2.

Mpodozis, C., and Ramos, V., 1990, The Andes of Chile and Argentina, *in* Ericksen, G.E., Pinochet, T.C., and Reinemund, J.A., eds., Geology of the Andes and its Relation to Hydrocarbon and Mineral Resources: Houston, Texas, Circum-Pacific Council for Energy and Mineral Resources, p. 59–90.

Olivares, B., Cembrano, J., Hervé, F., López, G., and Prior, D., 2003, Geometría y cinemática de la zona de cizalle Seno Arcabuz, Andes Patagónicos, Chile: Revista Geológica de Chile, v. 30, no. 1, p. 39–52, https://doi.org/10.4067/S0716-02082003000100003.

Pankhurst, R.J., and Rapela, C.W., 1995, Production of Jurassic rhyolite by anataxis of the lower crust of Patagonia: Earth and Planetary Science Letters, v. 134, p. 23–36, https://doi.org/10.1016/0012-821X(95)00103-J.

Pankhurst, R.J., Sruoga, J., and Rapela, C.W., 1993, Estudio geocronológico Rb-Sr de los complejos Chon Aike y El Quemado a los 47°30′ L.S., *in* XII Congreso Geológico Argentino y II Congreso Exploracion de Hidrocarburos, Actas IV: Mendoza, Argentina, Instituto Argentino del Petroleo, p. 171–178.

Pankhurst, R.J., Riley, T.R., Fanning, C.M., and Kelley, S.P., 2000, Episodic Silicic Volcanism in Patagonia and the Antarctic Peninsula: Chronology of Magmatism Associated with the Break-up of Gondwana: Journal of Petrology, v. 41, p. 605–625, https://doi.org/10.1093/petrology/41.5.605.

Pankhurst, R.J., Rapela, C.W., Loske, W.P., Márquez, M., and Fanning, C.M., 2003, Chronological study of the pre-Permian basement rocks of southern Patagonia: Journal of South American Earth Sciences, v. 16, p. 27–44, https://doi.org/10.1016/S0895-9811(03)00017-8.

Pankhurst, R.J., Rapela, C.W., Fanning, C.M., and Márquez, M., 2006, Gondwanide continental collision and the origin of Patagonia: Earth-Science Reviews, v. 76, p. 235–257, https://doi.org/10.1016/j.earscirev.2006.02.001.

Parada, M.A., López-Escobar, L., Oliveros, V., Fuentes, F., Morata, D., et al., 2007, Andean Magmatism, *in* Moreno, T., and Gibson, W., eds., The Geology of Chile: The Geological Society of London, p. 115–146.

Platt, J.P., 1983, Exhumation of high-pressure rocks: A review of concepts and processes: Terra Nova, v. 5, no. 2, p. 119–133, https://doi.org/10.1111/j.1365-3121.1993.tb00237.x.

Platt, J.P., 1986, Dynamics of orogenic wedges and the uplift of high-pressure metamorphic rocks: Geological Society of America Bulletin, v. 97, no. 9, p. 1037–1053, https://doi.org/10.1130/0016-7606(1986)97<1037:DOOWAT>2.0.CO;2.

Plunder, A., Agard, P., Chopin, C., Pourteau, A., and Okay, A.I., 2015, Accretion, underplating and exhumation along a subduction interface: From subduction initiation to continental subduction (Tavşanlı zone, W. Turkey): Lithos, v. 226, p. 233–254, https://doi.org/10.1016/j.lithos.2015.01.007.

Rapela, C.W., and Pankhurst, R.J., 1993, El volcanismo riolitico del noreste de la Patagonia: Un evento mesojurásico de corta duración y origen profundo, *in* XII Congreso Geológico Argentino y II Congreso Exploracion de Hidrocarburos, Actas IV: Mendoza, Argentina, Instituto Argentino del Petroleo, p. 791–497.

Richter, P.P., Ring, U., Willner, A.P., and Leiss, B., 2007, Structural contacts in subduction complexes and their tectonic significance: The late Palaeozoic coastal accretionary wedge of central Chile: Journal of the Geological Society [London], v. 164, no. 1, p. 203–214, https://doi.org/10.1144/0016-76492005-181.

Riley, T.R., Flowerdew, M.J., Pankhurst, R.J., Curtis, M.L., Millar, I.L., Fanning, C.M., and Whitehouse, M.J., 2017, Early Jurassic magmatism on the Antarctic Peninsula and potential correlation with the Subcordilleran plutonic belt of Patagonia: Journal of the Geological Society [London], v. 174, no. 2, p. 365–376, https://doi.org/10.1144/jgs2016-053.

Ring, U., and Brandon, M.T., 1999, Ductile deformation and mass loss in the Franciscan subduction complex: Implications for exhumation processes in accretionary wedges, *in* Ring, U., Brandon, M.T., Lister, G.S., and Willett, S.D., eds., Exhumation Processes: Normal Faulting, Ductile Flow and Erosion: Geological Society, London, Special Publication 154, p. 55–86, https://doi.org/10.1144/GSL.SP.1999.154.01.03.

Ring, U., and Layer, P.W., 2003, High-pressure metamorphism in the Aegean, Eastern Mediterranean: Underplating and exhumation from the Late Cretaceous until the Miocene to Recent above the retreating Hellenic subduction zone: Tectonics, v. 22, no. 3, 1022, https://doi.org/10.1029/2001TC001350.

Rondenay, S., Abers, G.A., and Van Keken, P.E., 2008, Seismic imaging of subduction zone metamorphism: Geology, v. 36, no. 4, p. 275–278, https://doi.org/10.1130/G24112A.1.

Sepúlveda, F.A., Hervé, F., Calderón, M., and Lacassie, J.P., 2008, Petrological and geochemical characteristics of metamorphic and igneous units from the allochthonous Madre de Dios terrane, southern Chile: Gondwana Research, v. 13, no. 2, p. 238–249, https://doi.org/10.1016/j.gr.2007.06.004.

Sepúlveda, F.A., Palma-Heldt, S., Hervé, F., and Fanning, C.M., 2010, Permian depositional age of metaturbidites of the Duque de York complex, southern Chile: U-Pb SHRIMP data and palynology: Andean Geology, v. 37, no. 2, p. 375–397, https://doi.org/10.5027/andgeoV37n2-a06.

Villa, I.M., De Bièvre, P., Holden, N.E., and Renne, P.R., 2015, IUPAC-IUGS recommendation on the half life of ^{87}Rb: Geochimica et Cosmochimica Acta, v. 164, p. 382–385, https://doi.org/10.1016/j.gca.2015.05.025.

Von Huene, R., and Lallemand, S., 1990, Tectonic erosion along the Japan and Peru convergent margins: Geological Society of America Bulletin, v. 102, no. 6, p. 704–720, https://doi.org/10.1130/0016-7606(1990)102<0704:TEATJA>2.3.CO;2.

Wakabayashi, J., 2015, Anatomy of a subduction complex: Architecture of the Franciscan complex, California, at multiple length and time scales: International Geology Review, v. 57, no. 5-8, p. 669–746, https://doi.org/10.1080/00206814.2014.998728.

Whitney, D.L., and Evans, B.W., 2010, Abbreviations for names of rock-forming minerals: American Mineralogist, v. 95, no. 1, p. 185–187.

Willett, S.D., Slingerland, R., and Hovius, N., 2001, Uplift, shortening, and steady state topography in active mountain belts: American Journal of Science, v. 301, no. 4-5, p. 455–485, https://doi.org/10.2475/ajs.301.4-5.455.

Williams, I.S., and Claesson, S., 1987, Isotopic evidence for the Precambrian provenance and Caledonian metamorphism of high grade paragneisses from the Seve Nappes, Scandinavian Caledonides. II: Ion microprobe zircon U-Th-Pb: Contributions to Mineralogy and Petrology, v. 97, p. 205–217, https://doi.org/10.1007/BF00371240.

Willner, A.P., 2005, Pressure-temperature evolution of a late Palaeozoic paired metamorphic belt in north-central Chile (34–35°30′S): Journal of Petrology, v. 46, no. 9, p. 1805–1833, https://doi.org/10.1093/petrology/egi035.

Willner, A.P., Hervé, F., Thomson, S.N., and Massonne, H.J., 2004a, Converging *P-T* paths of Mesozoic HP-LT metamorphic units (Diego de Almagro Island, southern Chile): Evidence for juxtaposition during late shortening of an active continental margin: Mineralogy and Petrology, v. 81, no. 1-2, p. 43–84, https://doi.org/10.1007/s00710-004-0033-9.

Willner, A.P., Glodny, J., Gerya, T.V., Godoy, E., and Massonne, H.J., 2004b, A counterclockwise *P-T-t* path of high-pressure/low-temperature rocks from the Coastal Cordillera accretionary complex of south-central Chile: Constraints for the earliest stage of subduction mass flow: Lithos, v. 75, no. 3-4, p. 283–310, https://doi.org/10.1016/j.lithos.2004.03.002.

Willner, A.P., Thomson, S.N., Kröner, A., Wartho, J.A., Wijbrans, J.R., and Hervé, F., 2005, Time markers for the evolution and exhumation history of a late Palaeozoic paired metamorphic belt in north-central Chile (34–35°30′S): Journal of Petrology, v. 46, no. 9, p. 1835–1858, https://doi.org/10.1093/petrology/egi036.

Willner, A.P., Sepúlveda, F.A., Hervé, F., Massonne, H.J., and Sudo, M., 2009, Conditions and timing of pumpellyite-actinolite-facies metamorphism in the early Mesozoic frontal accretionary prism of the Madre de Dios Archipelago (latitude 50°20′S; southern Chile): Journal of Petrology, v. 50, no. 11, p. 2127–2155, https://doi.org/10.1093/petrology/egp071.

Willner, A.P., Massonne, H.J., Ring, U., Sudo, M., and Thomson, S.N., 2012, *P–T* evolution and timing of a late Palaeozoic fore-arc system and its heterogeneous Mesozoic overprint in north-central Chile (latitudes 31–32 S): Geological Magazine, v. 149, no. 2, p. 177–207, https://doi.org/10.1017/S0016756811000641.

York, D., Hall, C.M., Yanase, Y., Hanes, J.A., and Kenyon, W.J., 1981, ^{40}Ar/^{39}Ar dating of terrestrial minerals with a continuous laser: Geophysical Research Letters, v. 8, no. 11, p. 1136–1138, https://doi.org/10.1029/GL008i011p01136.

Science Editor: Aaron J. Cavosie
Associate Editor: Chris Kirkland

Manuscript Received 22 July 2017
Revised Manuscript Received 19 January 2018
Manuscript Accepted 26 February 2018

Printed in the USA